The Formation Timescale Of Bulges In The BEARD Survey

Paula Sosa Guillén

Supervisors: Adriana de Lorenzo-Cáceres Rodríguez
& Jairo Méndez Abreu

Universidad de La Laguna

Master in Astrophysics

Final Master's Thesis

July 2023

Illustration by Celia Fernández Martín

Abstract

The study of galaxy evolution has been a subject of intense debate within the astronomical community. Interactions between galaxies and secular processes leave distinctive imprints on the properties of galaxies, contributing to their evolution. The ΛCDM cosmological model has successfully explained the large-scale structures of the universe, but the evolution of luminous structures, such as galaxies, differs from the formation history of dark matter halos. The BEARD project focuses on studying the metallicity and abundance properties of a sample of 66 massive bulgeless galaxies in the nearby universe to gain a better understanding of galactic evolution. The main objective of this work is to study the stellar populations properties in 27 galaxies from the BEARD sample, as well as to test the ability to obtain the age of galaxies in the spectral range of $4963 - 5443$ Å, which lacks lines sensitive to this parameter. The data used in this study were collected using the MEGARA IFU instrument with the MR-G gratins installed in the GTC. The method used was based on a python code implementing the pPXF algorithm adapted to our needs, and utilising the MILES SSP models. To ensure that our methodology used yields consistent results, mock spectra models were developed by modifying MILES models to mimmick the MEGARA data. These mock spectra were used to study two main parameters of our analysis: regularisation and signal-to-noise ratio. Additionally, these models made it possible to determine the error associated with the method, obtaining, in general, errors of $\pm$ 1 Gyr for ages younger than 4 Gyr, and errors always less than $\pm$6.2 Gyr for older ages. For metallicity, an error of $\pm$0.1 dex was obtained for all [M/H] values. The scientific results of this work were based on obtaining 21 maps of stellar populations along with their respective age-metallicity plane. Overall, a variety of results were found for the different bulges. We have analysed three galaxies of the sample which are NGC 5962, NGC 4405, and NGC 1087. Also, a comparative study was performed with the CALIFA survey (Méndez-Abreu et al., 2021) in order to shed some light on the bulge formation scenario. This study demonstrated the feasibility of determining stellar populations in spectra without age-sensitive lines, using analyses of mock spectral models. It is suggested that galactic bulges in the BEARD sample are mainly formed from material in the galactic disc and undergo internal secular evolution enriched with metals from previous generations of stars.

Resumen

El estudio de la evolución de las galaxias ha sido objeto de un intenso debate en la comunidad astronómica durante décadas. Las galaxias, como sistemas complejos, están sujetas a numerosos procesos y fenómenos que influyen en su formación y desarrollo a lo largo del tiempo. Las interacciones entre galaxias, la actividad nuclear, la formación de estrellas y las fusiones son solo algunos ejemplos de estos procesos que dejan huellas distintivas en las propiedades cinemáticas, químicas y fotométricas de las galaxias. Para comprender mejor la evolución galáctica, se han propuesto varios modelos y teorías. Uno de los modelos cosmológicos más exitosos es el modelo ΛCDM, que ha explicado con éxito las estructuras a gran escala del universo. Sin embargo, la evolución de las estructuras luminosas, como las galaxias, difiere de la historia de formación de los halos de materia oscura predichos por este modelo.

En las proximidades de nuestro universo, hemos observado un número de galaxias masivas que carecen de bulbo o tienen uno muy débil. Esta observación contradice tanto los escenarios de las galaxias tempranas tipo elípticas con bulbos prominentes, como el de las galaxias tardías (tipo disco). Por lo tanto, la implementación bariónica de la teoría del Universo ΛCDM presenta desafíos a escalas galácticas, especialmente en lo que respecta a la alta proporción de galaxias sin bulbo observadas en el Universo cercano.

En este contexto, el proyecto BEARD, se ha enfocado en el estudio de las propiedades de metalicidad y abundancia en una muestra de 66 galaxias masivas sin bulbo en el Universo cercano para profundizar en el conocimiento de la formación y evolución galáctica. De esta forma, se espera determinar la historia de formación de estas galaxias y compararla con simulaciones numéricas.

El objetivo principal de este trabajo de fin de máster es estudiar y analizar las poblaciones estelares en 27 galaxias de la muestra de BEARD, así como testear la capacidad de obtener la edad de las galaxias en el rango espectral 4963−5443 Å , carente de lineas sensibles a este parámetro.

Los datos utilizados en este estudio fueron recogidos mediante el uso del instrumento MEGARA instalado en el Gran Telescopio Canarias en el Observatorio del Roque de los Muchachos, en La Palma. Las observaciones se realizaron utilizando el grating VPH521-MR, con una resolución de 0.433 Å en la longitud de onda de 5213 Å y una dispersión de 0.122 Å/píxel. Después de un procesamiento adecuado de los datos, se seleccionó un binning de 2×2 para el análisis, lo cual permitió alcanzar un equilibrio entre la relación señal-ruido y la preservación de la estructura de los objetos observados.

El método utilizado en este estudio se basó en el desarrollo de un código en Python que implementa el algoritmo pPXF adaptado a las necesidades del proyecto. Se fijó la cinemática utilizando trabajos previos del grupo BEARD y se utilizaron los modelos SSP de MILES para llevar a cabo el análisis de las poblaciones estelares.

Con el fin de asegurar que el método utilizado nos permite obtener unos resultados coherentes se desarrollaron los espectros simulados, generados a partir de la modificación de MILES a los datos de MEGARA. Con estos se hizo un estudio de dos parámetros fundamentales en nuestro trabajo: la regularización y de la señal a ruido, pudiendo determinar que el mejor factor de regularización encontrado fue 5 y que la señal a ruido mínima requerida para el análisis de los datos es 15. Además, con estos modelos fue posible determinar el error asociado al método, obteniendo en general, para edades menores de 4 Gyr errores de ±1 Gyr, y para edades mayores errores siempre menores a ±6.2 Gyr. Para la metalicidad, se obtuvo un error de ±0.1 dex para todo el rango de [M/H].

Los resultados científicos obtenidos en este estudio se basaron en la obtención de 21 mapas de poblaciones estelares, tanto para las edades como para las metalicidades, junto con sus respectivos planos de edad-metalicidad. Se observó una variedad de resultados para los diferentes bulbos de las galaxias estudiadas, en concreto se analizaron en profundidad las galaxias NGC 5962, NGC 4405 y NGC 1087. Además se comparó la muestra de galaxias con los resultados obtenidos por de Lorenzo-Cáceres et al. (en preparación) , utilizando datos del survey de CALIFA (Méndez-Abreu et al., 2021), con el objetivo de determinar el escenario de evolución de los bulbos galácticos.

En conclusión, este estudio demostró la viabilidad en la determinación de las poblaciones estelares en espectros que no presentan líneas sensibles a la edad, confirmado mediante el análisis de los espectros simulados. Fue posible hacer un estudio detallado de las estructuras y la evolución de las galaxias en análisis, pudiendo determinar explicitamente para NGC 5962, NGC 4405 y NGC 1087 sus picos de formación estelar y gradientes de metalicidad. Además, se infiere un escenario de formación de los bulbos galácticos jóvenes, donde estos se generan a partir de material del disco galáctico, experimentando una evolución secular interna enriquecida en metales provenientes de generaciones previas de estrellas. Estos hallazgos contribuyen al entendimiento de la evolución de las galaxias sin bulbo y aportan información importante para la construcción de modelos teóricos más precisos y completos de la formación y evolución de las galaxias en el Universo cercano.

Contents

1 Introduction

1.1 Scientific context

The human fascination with understanding the sky emerges almost simultaneously with humanity itself. Consequently, following the discovery of the first systems external to the Milky Way, it became imperative to define and differentiate the variety of systems encountered in the universe.

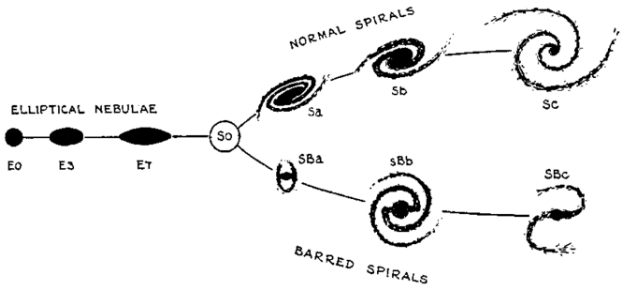

Figure 1: Morphological classification according to the Hubble sequence (Hubble, 1926). From left to right elliptical, lenticular, and spiral galaxies.

In 1926, the first morphological classification of galaxies was published by Hubble. Depicted in Figure 1, it shows the so called *Hubble diagram* that divides regular galaxies into three main types: ellipticals, spirals, and lenticulars each with specific subtypes. This classification is based on criteria such as the galaxy's light concentration, isophotes, presence of a bar, prominence of the bulge, or openness of spiral arms. However, as scientific knowledge progressed, more detailed morphological classifications began to be published, such as De Vaucouleurs' classification (De Vaucouleurs, 1959), which includes irregular galaxies and intermediate types between spirals and irregulars. Nonetheless, all these classifications revealed deficiencies when it came to making quantitative morphological divisions. Therefore, from that point onward until the present day, the scientific community has been striving to derive physical properties that can divide galaxies using more robust methods. Consequently, technics such as photometric decompositions, kinematic analyses, studies of stellar populations, or the presence of gas in the medium are implemented in order to determine the nature and characteristics of a galaxy.

In this context, the study of galaxy evolution has been a subject of intense debate within the astronomical community. On one side, galaxies might have evolved under the influence of other close galaxies, leading to complex interactions and a lack of isolation, particularly during the early stages of the universe when it was denser. On the other hand, secular processes (Kormendy and Kennicutt Jr, 2004), such as nuclear activity, star formation, and mergers, leave distinct imprints on the kinematic, chemical, and photometric properties of galaxies, contributing to their diverse evolution (Toomre, 1977). The understanding of these mechanisms is crucial in unravelling the riddle of galaxy evolution.

The widely accepted cosmological model, ΛCDM (Λ Cold Dark Matter), has successfully explained the large-scale structures of the universe. According to this model, dark matter halos convert potential energy into kinetic energy, leading to the formation of galaxies through the cooling of baryons (White and Rees, 1978). However, the evolution of luminous structures, such as galaxies, deviates from the assembly history of dark matter halos.

The formation of ETGs follows a two-phase process. Initially, a collapse of gas-rich material occurs, leading to the formation of a dense stellar core. This rapid formation process, known as gas compaction, is facilitated by the growth of supermassive black holes (SMBH hereafter) at the centres of these galaxies. Subsequently, the evolution of ETGs involves the dry accretion of satellites and occasional major mergers (see Oser et al. (2010)). These processes play a crucial role in shaping the overall properties of massive ETGs, being in coherence with their observed scaling relations (such as the mass Faber-Jackson relation $M \propto \sigma^4$ (Costantin

et al., 2020)). Prominent bulges of massive spiral galaxies shows similar relations. This suggests a comparable formation process shared with ETGs, wherein the bulge forms early in the history of the galaxy, preceding the development of the disc. The close relationship between the growth of BH and the formation of bulges further supports this idea (Kormendy and Gebhardt, 2001).

In contrast, late-type galaxies undergo gradual secular processes during their disc evolution, leading to the formation of smaller and less massive bulges (Kormendy and Fisher, 2008). These secular processes contribute to the development of disc-like structures in the central regions of late-type galaxies, which deviate from the fundamental virial relations observed in ETGs and large bulges. The internal redistribution of angular momentum within the disc-like component and the gradual infall of gas result in slower growth of the SMBH within these galaxies. This gradual and continuous formation of small bulges in late-type galaxies adds complexity to the co-evolution of SMBH and bulges, further highlighting the diverse pathways in galaxy evolution (Kormendy and Kennicutt Jr, 2004).

In the close vicinity of our universe, we have observed a number of massive galaxies that lack a prominent bulge or possess a faint one. This observation contradicts both the scenarios of ETG (with prominent bulges) and late-type galaxies (lacking massive bulges). Therefore, the baryonic implementation of the ΛCDM Universe theory presents challenges at galactic scales, particularly regarding the high fraction of bulgeless galaxies observed in the nearby Universe. According to this theory, violent merger processes should destroy stellar discs and form massive bulges (Scannapieco et al., 2009).

To unravel the nature of the central regions of galaxies, it is essential to study the spatially resolved properties of their stellar populations. Radial profiles of stellar metallicity and the relative abundance of [α/Fe] elements provide valuable information about the formation processes. Theoretical models suggest that monolithic collapse scenarios produce strong negative metallicity gradients (Eggen et al., 1962), while galaxy mergers tend to dilute these metallicity (Di Matteo et al., 2009). Secular processes may contribute to the creation of new structures in galaxy centres, leading to younger, more metal-rich components with lower abundances of [α/Fe] elements. Determining the origin of the central regions of massive bulgeless galaxies, whether through violent processes at high redshift or secular mechanisms, is crucial for understanding their formation and their implications for the ΛCDM theory.

The study of galaxy evolution remains a complex and intriguing field of research. With the help of integral field spectroscopy and theoretical models, researchers continue to solve the mechanisms and processes that shape galaxies over cosmic timescales. By understanding the interplay between internal secular processes, environmental influences, and hierarchical clustering, we can gain deeper insights into the formation and evolution of galaxies and address the challenges posed by the baryonic implementation of the ΛCDM theory.

The BEARD (Bulgeless Evolution And the Rise of Discs) project, as which the current TFM take part on, focuses on measuring the stellar metallicity, age, and [α/Fe] abundance properties in the central regions of a volume-limited sample of 66 massive bulgeless galaxies in the nearby Universe. This research project contributes to our overall comprehension of galaxy evolution and provides essential constraints for refining theories and models, shedding light on the broader understanding of galaxy evolution in the nearby Universe.

This master's thesis aims to contribute to the development of the scientific issues surrounding bulgeless galaxies and their evolution over time. To achieve this, this introductory section will mention some of the most important concepts regarding stellar populations and their study. The BEARD project will also be presented. Subsequently, the objectives to be pursued will be discussed, followed by the methodology employed. This will include an explanation of the data acquisition using MEGARA, as

well as the pre- and processing data phases. Furthermore, the main technical development tools, namely pPXF (Cappellari, 2017) and the MILES models (Vazdekis et al., 2015), will be introduced. Following this, a section will be dedicated to the analysis of mock models, which are created to ensure reliable and robust results. Finally, the obtained results regarding ages and metallicities for the galaxies in the sample will be presented and compared with the literature to end concluding our work.

1.2 Theoretical concepts

Studies can be conducted on both resolved and unresolved stellar populations. Resolved stellar populations refer to situations where information about individual stars in a galaxy can be obtained, such as in the case of the Milky Way and its satellites (the only systems in which such detailed analysis is currently feasible, e.g. Ruiz-Lara et al. (2015) Ruiz-Lara et al. (2018)). However, it is worth noting that advancements in technology have allowed for the analysis of certain types of stars within nearby galaxies. Conversely, studies can also be undertaken on unresolved populations, which involve studying the galaxy as a collective of stars. This work falls under the latter category, examining the galaxy as a stellar ensemble.

This master thesis study follows the principles of extragalactic archaeology with a fossil approach. Through the utilisation of integral field spectroscopy, the galaxy is analysed and spatially resolved into its distinct components (bulge, disc, bars, ...), enabling the acquisition of their star formation histories. By doing so, it becomes feasible to determine the chronological emergence of stars within different regions of the system. However, it is crucial to acknowledge a noteworthy limitation of this method, namely the potential migration of stars. The fossil approach does not account for the dynamic evolution of the galaxy, thereby resulting in the possibility that stars may have relocated over time, yet still being attributed to the element under current investigation. This phenomenon is particularly noticeable in barred galaxies, which exhibit significant stellar motion. Additionally, it is important to consider the influence of interactions between galaxies or the cosmic web, which can alter the composition of a system, consequently modifying its star formation history.

In this context, several significant concepts are cited (Kennicutt Jr et al., 1998):

- Star Formation History (SFH): Refers to the temporal pattern of star formation within a galaxy, indicating the quantity of stars that have formed over time.
- Star Formation Rate (SFR): Denotes the rate at which stars are currently being formed.
- Spectral Energy Distribution (SED): Represents the spectrum of a galaxy. By analysing the SED, it is possible to derive information about the stellar populations within the galaxy, like their age and metallicity.
- Single Stellar Population (SSP): Refers to the spectrum of a group of stars that formed simultaneously. This population is characterised by a specific age and metallicity. SSPs are constructed as models that facilitate the comparison of real data with predicted outcomes.

Ingredients for building SSP models

- Stellar Libraries: These are a collection of stellar spectra obtained either through theoretical or observational means (Conroy, 2013). The study of stars is known to be complex, encompassing various stages of evolution and specific phenomena such as rotation or pulsation. Therefore, providing a theoretical definition for a stellar library is highly intricate. Consequently, relying on observational libraries is highly advantageous as they take into account specific processes occurring during stellar life. However, all observational libraries are derived from stars within the Milky

Way, limiting the data to the solar neighbourhood and consistently considering the same metallicities and environments.

– Isochrones: An isochrone represents the position of stars with a common age in the Hertzsprung-Russell diagram. Various widely-used isochrone tables are present in literature. Currently, the most popular models are the Padova models (Bertelli et al. (1994), Marigo et al. (2008)) and the BaSTI models (Pietrinferni et al., 2004). However, other such as the Genova (Schaller et al., 1992), Dartmouth (Dotter et al., 2008)), or Regina isochrone models (VandenBerg and Bell (1985), VandenBerg et al. (2006)) also exist, catering to specific characteristics.

– Initial Mass Function (IMF): It quantifies the number of stars formed per unit mass. Different IMF models have been proposed, such as Salpeter (1955), Scalo (1986), Kroupa (2001), and Chabrier (2003).

Thus, with stellar libraries, IMF, and isochrones, it is possible to generate single stellar population models. These, along with considerations about dust and chemical evolution of the system, allow for the determination of a spectral energy distribution, see Figure 2.

Mass & Luminosity weighted

In the field of stellar population studies, the terms *mass-weighted* and *luminosity-weighted* refer to different approaches used to average stellar population properties within a galaxy, taking into account the contributions from different stars.

The *mass-weighted* approach entails assigning the weight to the amount of mass within a stellar population. In other words, the stellar properties with a higher mass will have a greater influence on the weighted average. On the other hand, the *luminosity-weighted* approach assigns higher weight to the more luminous stars. Here, the younger stars will contribute more significantly to the averaged properties of the galaxy.

Z$-\sigma_\star$ degeneracy

The Z$-\sigma_\star$ degeneracy arises from the fact that both, metallicity and velocity dispersion, can impact the width of a spectrum line. This degeneracy complicates the precise distinction between the contribution of each of these factors. Moreover, these parameters are not the only contribution to the broadness of the spectrum, others such as IMF or the presence of dust also have an influence.

It is crucial to note that this spectral alteration is a subtle effect. A detailed and meticulous analysis is required to properly separate these influences and understand their impact on measurements and data interpretations.

1.3 The BEARD project

The BEARD project was born based on the scientific context exposed in Section 1.1. Nowadays, galaxies with $\log\left(\frac{M_\star}{M_\odot}\right) > 10.5$ are supposed to have experienced, at least, a major merger during their lives, forming important structures in their centre and destroying or heating up discs (White and Rees, 1978). Therefore, the existence of massive bulgeless galaxies in the nearby Universe poses a challenge for the theory of hierarchical galaxy formation. This study could be a perfect opportunity to test the Λ Cold Dark Matter Universe.

The specific scientific objectives presented by the BEARD project are focused on determining the merger and star formation history of bulgeless galaxies and their evolution, as well as comparing the results with the numerical simulations. This will allow the hierarchical models to be challenged. They divide the scientific objectives into four main groups: (1) The nature of the structures at the centre of bulgeless galaxies, (2) the low surface brightness features of bulgeless galaxies, (3) the stellar populations and star formation of bulgeless galaxies, and (4) the theory and numerical simulations.

The BEARD sample consists of a set of 66 bulgeless massive galaxies ($\log\left(\frac{M_\star}{M_\odot}\right) > 10$) in

the nearby universe (D $<$ 40 Mpc). The observations include deep optical imaging to study the low surface brightness structures with the Wide Field Camera at the Isaac Newton Telescope (INT); narrow-band photometry around the Hα line to derive the SFR using in the IO:O instrument at the Liverpool Telescope; long-slit spectroscopy to observe the stellar population gradients with DOLORES at the Telescopio Nazionale Galileo, and integral-field spectroscopy to derive the faintest and embedded nuclei in bright discs using MEGARA at the Gran Telescopio de Canarias. Observations have been possible thanks to the International Time Programme (ITP) awarded by the International Scientific Committee (CCI) during 2 consecutive years.

All sample galaxies are taken from the SDSS-DR13 spectroscopic catalogue, and satisfy the following conditions:

i. Inclination i $<$ 60 degrees: allowing a good photometric definition of the central region and limiting the dust effects.

ii. Concentration of C $= \frac{R_{90}}{R_{50}} > 2.5$ (dominate by late-type disc galaxies (Graham and Driver, 2005)).

iii. Petrosian radius $> 10''$: to have sufficiently large galaxies.

To achieve the past merger history of nearby galaxies it is essential to make a multidisciplinary study. This is the reason that leads the BEARD team to an international context, having 25 researchers from seven different countries, led by Jairo Méndez-Abreu (IAC, PI). We count with professionals in stellar and gas kinematics, stellar populations, star formation, galaxy evolution, and others.

BEARD also involves the participation of several students who are either gaining practical experience or working on their Master's final thesis. Of particular concern to me, as a student at the University of La Laguna, is the last case mentioned. I contribute specifically to the stellar populations and star formation area as well as to the nature of the structures at the centre of bulgeless galaxies.

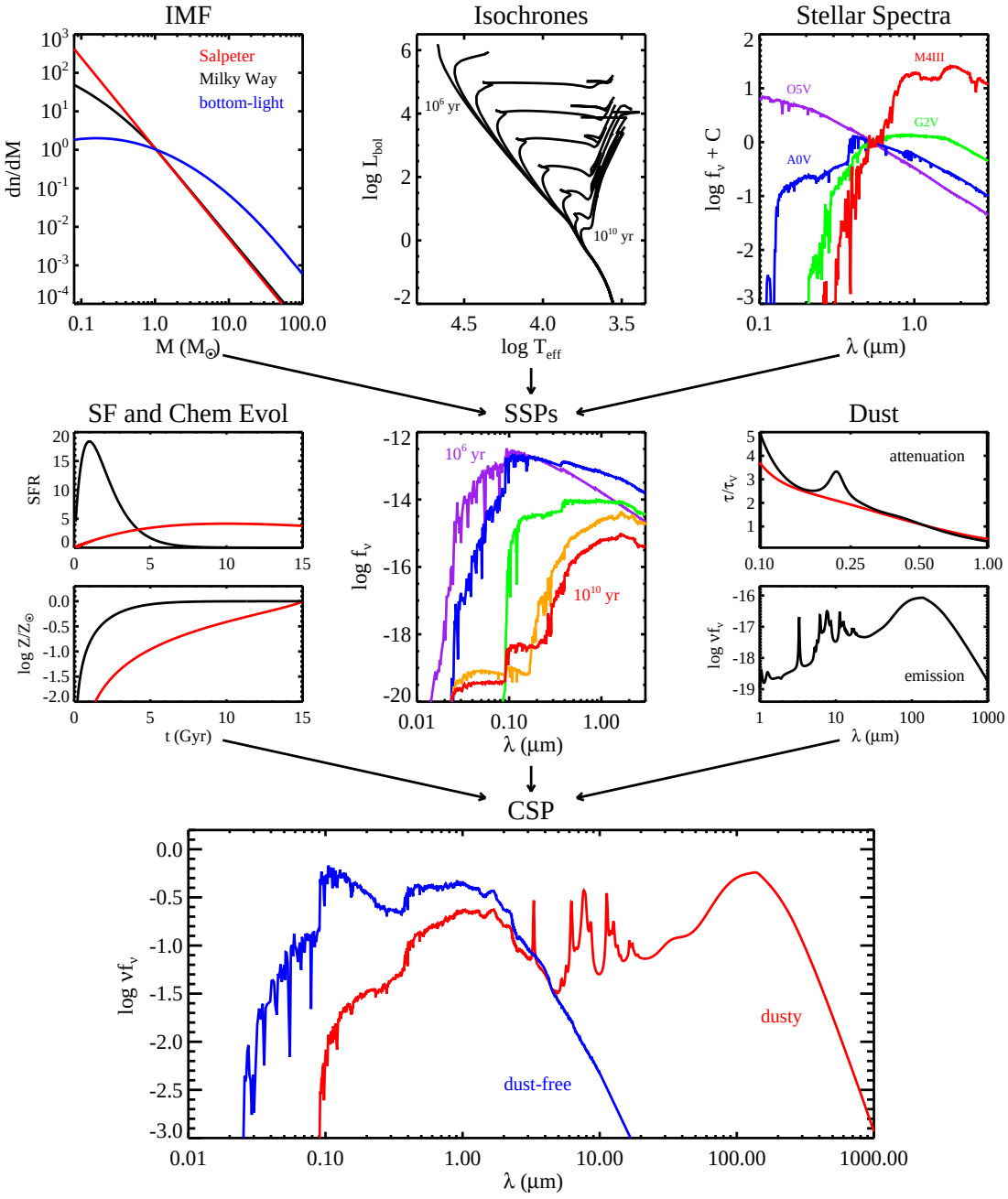

Figure 2: Overview of the stellar population synthesis technique. The upper panels highlight the ingredients necessary for constructing simple stellar populations (SSPs): an IMF, isochrones for a range of ages and metallicities, and stellar spectra spanning a range of T_{eff} , L_{bol}, and metallicity. The middle panels highlight the ingredients necessary for constructing composite stellar populations (CSPs): star formation histories and chemical evolution, SSPs, and a model for dust attenuation and emission. The bottom row shows the final CSPs both before and after a dust model is applied. *Figure and caption taken from Conroy (2013).*

2 Objectives

From a technical perspective, the objective of this project is to gain knowledge and proficiency in the various tools employed in professional integral field spectroscopy. Consequently, the goal is to modify and execute the pPXF fitting code for compatibility with the BEARD MEGARA data. By utilising Python and the pPXF package, the aim is to develop a code that can extract the stellar populations from a MEGARA MR-G data cube. This implies working with the instrument's spatial and spectral resolutions, as well as ensuring accurate data integration within the program. Furthermore, it encompasses the manipulation of stellar libraries, specifically MILES in this instance.

From a scientific standpoint, the primary aim of this study is to obtain the age of galaxies within the MEGARA wavelength range. Unfortunately, this range, spanning from 4963 – 5443 Å, lacks the capability to detect Balmer lines, which are highly indicative of age, with Hβ at 4861.33 Å being the closest observable line. Consequently, accurately calculating the stellar populations becomes exceedingly challenging. Hence, this investigation seeks to determine to which extent we can reliably recover this parameter and assess the associated error in population determination. In order to achieve this, a meticulous methodology (outlined in section 5) is developed to ensure the robustness of our findings. This methodology involves the generation of mock models derived from the MILES models, mimicking the observed properties of our MEGARA data. Subsequently, we employ pPXF on these mock models to acquire results, and the analysis of these outcomes will establish the feasibility of the developed code.

Once we have accomplished the aforementioned goals, we will be well-prepared to tackle the second scientific objective, which involves generating resolved age and metallicity maps. These maps will serve as valuable tools for initiating an in-depth scientific discussion regarding the morphological and structural implications of the BEARD massive bulgless galaxies.

Certainly, the analysis conducted in this work is based in a robust theoretical framework that underpins the results and discussions presented. Therefore, a significant portion of this Master's thesis has been dedicated to studying concepts pertaining to both the galactic and extragalactic domains as well as the extension of prior knowledge concerning the physics of stellar populations and their evolutionary processes over time. This comprehensive theoretical foundation forms a vital basis for the findings and interpretations put forwards in this study.

3 Methodology and Data Processing

3.1 MEGARA Data obtention

To observe and obtain information about many different astronomical objects, the scientific community has developed MEGARA, a multi-spectrograph of high spectral resolution integrated into the Gran Telescopio de Canarias (GTC hereafter) in the Roque de Los Muchachos (ORM hereafter), La Palma.

MEGARA is a versatile instrument operating in the wavelength range between 0.4 and 1 μm. It is placed in the Nasmyth A platform of GTC focus, a stable place where the instrument assembly can be kept stabilised (de Paz et al., 2012). The instrument has two modes: the integral field unit mode (IFU), and the multi-object spectrograph mode (MOS). Both systems can provide low, medium, and high spectral resolutions (R $\sim 5500, 1200, 20000$), which are LR, MR, and HR respectively with a spaxel size of $0''.62$ (de Paz et al., 2016).

- The Integral-Field Unit (IFU) mode has a fibre system with a field of view (FoV hereafter) of $12''.5 \times 11''.3$. It is composed of 567 fibres of 100 μm installed at the optical axis centre with 8 mini-bundles devoted to sky/background emission.
- The Multi-Object Spectroscopy (MOS) mode has 644 fibres all around the IFU's fibres packaged in 92 sub-assemblies. It covers a FoV of $3'.5 \times 3'.5$ in the sky.

The data used in this work were obtained with the IFU mode of MEGARA instrument, allowing us to analyse the central region of 27 BEARD galaxies in detail. The data was taken during $2019 - 2022$.

The grating used in the observations was the VPH521−MR with the setup MR−G. It works in the wavelength range between $4963 - 5443$ Å, with a resolution of 0.433 Å at 5213 Å, and a dispersion of 0.122 Å/px. Although the spaxel size is $0''.62$, we use a resampling to square spaxels, which is done with a spaxel size of $0''.4$. All data had an on-target exposure of $1000 - 1200$ seconds, but NGC 1090 with 850 seconds. This technical configuration provides the signal-to-noise (S/N hereafter) per spectral resolution element needed to archive the BEARD scientific goal. Table 1 shows some technical and scientific information for each galaxy.

3.2 Pre-processing phase

Basic data reduction was carried out by the BEARD group with the MEGARA data reduction pipeline (DRP) v0.12.0, following the Chamorro-Cazorla et al. (2023) guidelines. They remove the bias level present in the images, involving overscan correction and trimming to match the spaxel sizes. Also, they have done the calibration of the fibres, to ensure proper alignment of the paths they follow to the detector, the wavelength calibration, and the fibre-specific calibration to account for transmission variation as a function of wavelength. Additionally, they have taken into account the flux calibration, performed using spectra of standard stars available in the ESO spectrophotometric database. Finally, the identification and removal of diffuse light caused by the presence of the moon in some exposures have been performed.

Once this has been done, a 3D datacube was obtained, consisting of two spatial and one spectral dimension.

3.3 Processing phase

The BEARD group had computed the binning and the stellar kinematics associated with each galaxy.

To increase the signal-to-noise ratio (S/N hereafter) for each spaxel, they performed binning by averaging the spectrum within box-shaped regions of sizes 1, 2, and 3 spaxels. Additionally, a Voronoi Binning method was employed, following the approach by Cappellari and Copin (2003). Adjacent spaxels were combined until achieving an average continuum S/N of 15.

Table 1: Sample of galaxies used to perform this work. *First column*: Name of the 27 galaxies. *Second and third column*: Coordinates of each object in the sky. *Fourth column*: Total exposure time taken during each observation. *Fifth and sixth column*: Bulge mass and radius by Zarattini et al. (in preparation), galaxies without bulge data are defined as pure bulgeless.

Galaxy	Right Ascension [hh : mm : ss]	Declination [deg : mm : ss]	Exposure time [s]	Bulge mass [$M_\odot$]	Bulge radius [″]
IC 3392	12 : 28 : 43.309	+14 : 59 : 58.202	1200.0	5.21×10^8	2.97
NGC 0514	01 : 24 : 04.050	+12 : 55 : 02.896	1200.0	9.06×10^8	4.39
NGC 1087	02 : 46 : 25.180	−00 : 29 : 55.277	1200.0	1.81×10^8	1.74
NGC 1090	02 : 46 : 33.975	−00 : 14 : 49.769	850.0	1.87×10^8	3.41
NGC 2543	08 : 12 : 58.062	+36 : 15 : 16.566	1200.0	1.15×10^9	0.99
NGC 2701	08 : 59 : 06.040	+53 : 46 : 17.918	1200.0	-	-
NGC 2742	09 : 07 : 34.046	+60 : 28 : 46.036	1200.0	2.03×10^8	2.48
NGC 2776	09 : 12 : 14.605	+44 : 57 : 17.430	1200.0	2.84×10^9	3.44
NGC 3294	10 : 36 : 16.296	+37 : 19 : 28.580	1200.0	7.96×10^8	3.09
NGC 3338	10 : 42 : 07.588	+13 : 44 : 49.135	1200.0	1.94×10^9	5.38
NGC 3430	10 : 52 : 11.315	+32 : 57 : 01.399	1200.0	4.56×10^8	2.30
NGC 3486	11 : 00 : 23.943	+28 : 58 : 30.449	1000.0	1.17×10^9	3.20
NGC 3614	11 : 18 : 21.055	+45 : 44 : 53.466	1200.0	5.27×10^8	2.87
NGC 3756	11 : 36 : 47.935	+54 : 17 : 36.700	1200.0	1.66×10^8	2.08
NGC 3780	11 : 39 : 22.440	+56 : 16 : 14.265	1200.0	1.91×10^9	3.36
NGC 3810	11 : 40 : 58.665	+11 : 28 : 16.000	1000.0	1.08×10^9	3.96
NGC 3938	11 : 52 : 49.345	+44 : 07 : 14.600	1000.0	8.27×10^8	3.59
NGC 4062	12 : 04 : 03.735	+31 : 53 : 44.800	1200.0	1.53×10^8	4.06
NGC 4405	12 : 26 : 07.054	+16 : 10 : 51.600	1200.0	1.91×10^8	1.56
NGC 5313	13 : 49 : 44.255	+39 : 59 : 05.101	1200.0	5.05×10^9	2.16
NGC 5320	13 : 50 : 20.295	+41 : 21 : 58.301	1200.0	8.44×10^8	3.01
NGC 5347	13 : 53 : 17.694	+33 : 29 : 27.001	1000.0	1.45×10^9	1.41
NGC 5633	14 : 27 : 28.305	+46 : 08 : 47.602	1200.0	-	-
NGC 5899	15 : 15 : 03.296	+42 : 02 : 59.248	1200.0	5.23×10^9	2.35
NGC 5962	15 : 36 : 31.595	+16 : 36 : 28.102	1200.0	-	-
NGC 6070	16 : 09 : 58.605	+00 : 42 : 33.102	1200.0	1.84×10^9	3.49
UGC 04375	08 : 23 : 11.336	+22 : 39 : 52.866	1200.0	7.33×10^8	4.84

For each binning configuration, they obtained velocity, velocity dispersion, and higher-order Gauss-Hermite moments (h3 and h4) maps for the entire galaxy sample. To characterise the stellar kinematics, they utilised the Penalised PiXel-Fitting routine (Cappellari and Emsellem (2004), Cappellari (2017)) with the HR- PYPOPSTAR library (Millán-Irigoyen et al., 2021), incorporating 424 different single stellar populations with a better spectral resolution than MEGARA (0.1 Å) . The spectra fitted while masking the emission lines, specifically [O III] at 5198 Å and, in certain galaxies, the [N I] doublet at 5200 Å (Ferland et al., 2012).

3.3.1 Binning scheme selection

After the processing and preparation of the MEGARA data for analysis, the next step involved selecting the most appropriate binning approach based on the specific scientific objectives.

The criteria follow to choose the binning was the S/N ratio of each galaxy: the larger this ratio is, the better the subsequent analysis can be, but more spatial resolution is lost. In this context, three main aspects need to be taken into account:

i. Maintain the structure and morphology of the galaxies.

ii. Prioritise the region where the bulge is located, as we are more interested in it than in the outer parts (which may belong to the disc, bar, or other surrounding structures).

iii. Have the highest possible S/N as long as the binning is the most suitable for the global galaxies.

To identify the bulge region of the datacubes we have used the photometric decomposition performed by the BEARD team in Zarattini et al. (in preparation). They provide the bulge effective radius in arcseconds for the BEARD galaxy sample. The galaxies NGC 2701, NGC 5633, and NGC 5962 are classified as pure bulgeless, therefore we select a central component of 1″ of radius to make the analysis.

We made 4 different S/N maps (corresponding to the 4 binning) for the 27 galaxies in order to compare the different values obtained in the binned data. The signal (S hereafter) was obtained, for each galaxy, with the average value of all the wavelength range per spaxel in the datacubes, masking [O III] at 5198 Å and the [N I] doublet at 5200 Å. The noise (N hereafter) was calculated as the standard deviation of the residual between the datacubes and the best fit stellar kinematics model. At the end of the process we retrieve two maps (S & N) covering the MEGARA FoV. The result of these S/N maps are shown in the Figure 3 for NGC 5962, where we have represented the bulge radius as a black line and in coloured contours the S/N $= 15, 20, 25$ per resolution element.

We finally decided to use the 2×2 binning, as it provides a considerable S/N ratio in the central region of the galaxy and it conserves the structure in most cases.

3.4 MILES SSP models

To ensure the proper utilisation of pPXF, it is essential to employ a set of SSP models. We have use those of MILES [1], these models can be generated using different initial mass functions (IMF), isochrones and a star library.

Presently, with regard to libraries, the scientific community has developed some of them, including STELIB (Le Borgne et al., 2003), MILES (Sánchez-Blázquez et al., 2006) (Falcón-Barroso et al., 2011), ELODIE (Prugniel and Soubiran, 2001), MaStar (Yan et al., 2019), or X-Shooter (Chen et al., 2014), (Verro et al., 2022). These libraries serve as valuable resources for conducting accurate analyses and enhancing the reliability of results achieved through pPXF.

[1] http://miles.iac.es/

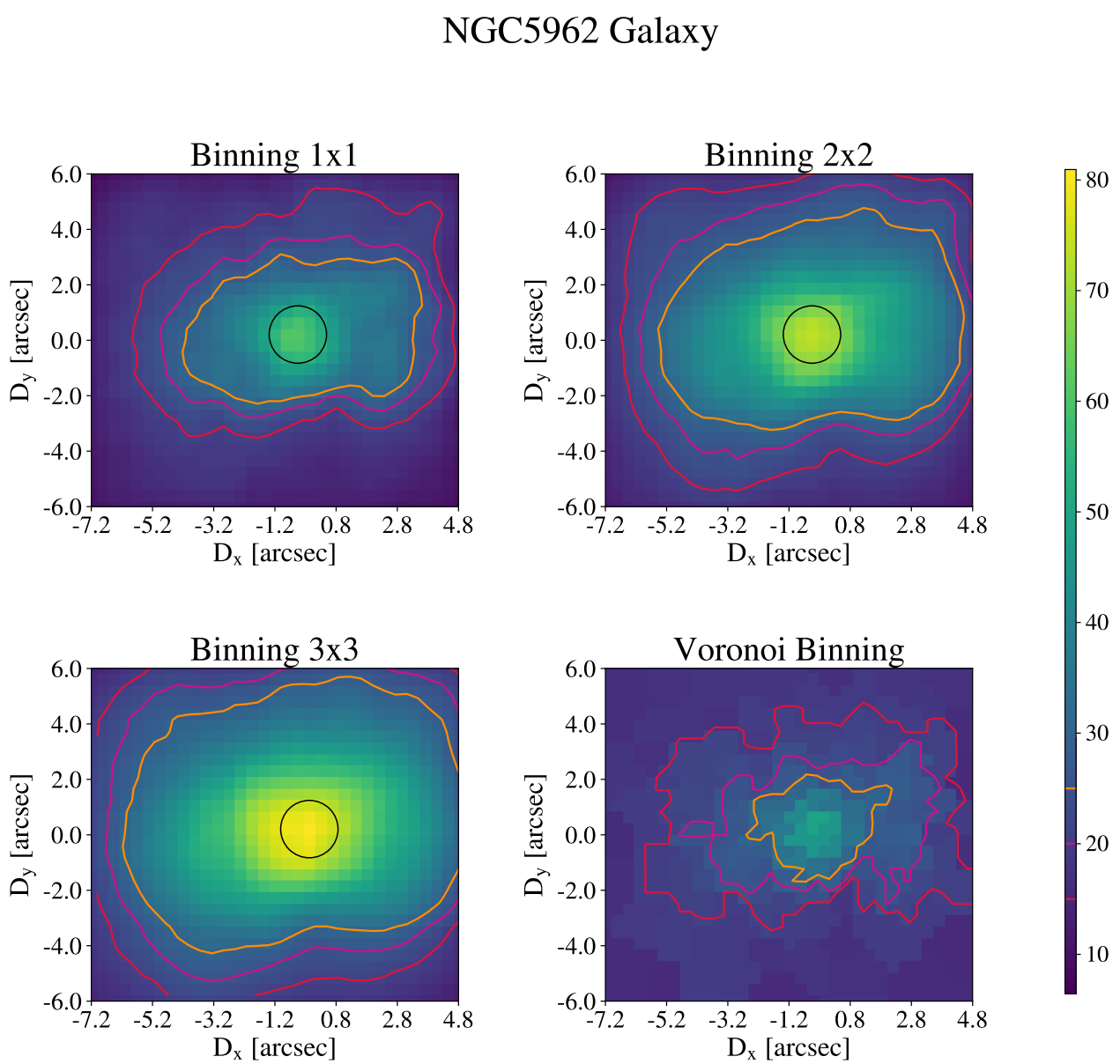

Figure 3: Signal-to-Noise maps for NGC 5962. The colour scale is given on the right side of the whole figure, and it provides the value of S/N for each of the maps. In black, we represent the bulge radius, which is 1″ (considered by us, as is a pure bulgeless galaxy). In red, purple, and orange we have selected the contours of S/N= 15, 20, and 25 respectively. *Top-left panel*: 1×1 binning. *Top-right panel*: 2×2 binning. *Bottom-left panel*: 3×3 binning. *Bottom-right panel*: Voronoi binning. 1″ = *164.8 pc.*

For this Master's thesis, we utilised the MILES (MIL EStrellas) library, which were published in Sánchez-Blázquez et al. (2006). We have chosen this particular library over others because it is a semi-empirical library specifically designed for the calculation of stellar populations, which is our primary objective in this project.

This library encompasses approximately 1000 stars, spanning a wide range of atmospheric parameters. The spectra were acquired using the 2.5m INT telescope at The Roque de Los Muchachos Observatory and cover a wavelength range between $3525 - 7500$ Å with a spectral resolution of 2.50 Å (FWHM). Additionally, the library provides spectra for the near-IR Ca II triplet, spanning $8350 - 9020$ Å with a spectral resolution of 1.5 Å (FWHM), as well as SSP models. The substantial enhancements of this library compared to previous ones used in population synthesis models include improvements in spectral resolution, spectral type coverage, flux calibration accuracy, and the number of stars. The spectra in both libraries exhibit a very high signal-to-noise ratio, typically surpassing 100, with some exceptions (see Vazdekis et al. (2015)). The spectra are similar to those shown in the Figure 4.

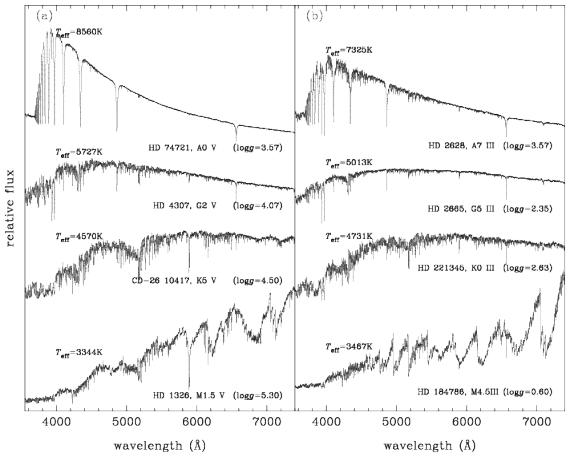

Figure 4: Examples of spectra from some of the stars used for the development of the MILES models. *Obtained from the MILES webpage of the IAC.*

In particular, for this study, we use SSP models with a bimodal IMF with a logarithmic slope for the massive star segment and BASTI scaled-solar isochrones (Pietrinferni et al., 2014) (Vazdekis et al., 2015).

The templates employed in pPXF are referred as *base models*. In Vazdekis et al. (2015) they explain how these models are computed and developed. The *base models* assume [M/H]=[Fe/H] and they cover a range of [M/H] from −2.5 to +0.4 and an age range from 0.03 to 14 Gyr. All of them were employed to fit the data, resulting in 53 values for age and 12 values for metallicity.

3.5 pPXF code

This final master's thesis is based on the stellar population studies of a given galaxy set. To carry out this work it has been used Python algorithms that have made possible the correct development of the main objective of the study. The most important of which has been pPXF.

To extract the gas and stellar kinematics, the stellar populations and the chemical composition of objects in the Universe, the Penalized PiXel-Fitting (pPXF) [2] code by Michael Cappellari has been performed (Cappellari, 2022) (Cappellari, 2017). Although initially constructed for the calculation of stellar kinematics, this algorithm was later adapted to also recover stellar populations, which is the purpose it has been given in this project.

The pPXF algorithm searches for the best linear combination of reference spectra (SSP, which contain information about the known stellar features) that match the observed spectra by assigning a certain weight to each of the SSPs.

In order to accomplish this objective, the algorithm undergoes multiple iterations until it discovers the optimal combination. Within each iteration, the χ^2 value, which signifies the degree of agreement between the observed spectra and the reference one, is computed to determine the fit that minimizes this metric.

Furthermore, pPXF adopts a penalised ap-

[2] https://pypi.org/project/ppxf/

proach to improve the accuracy and stability of the results by incorporating constraints and penalties. It ensures the avoidance of unphysical or unstable solutions during the analysis process. Penalties are utilised to govern specific established parameters. Among the most crucial fixed parameters are the kinematics (V, σ, h3, h4), the multiplicative polynomial, and the regularization factor.

The stellar kinematics were first determined using high-resolution stellar models in a preliminary step (see Section 3.3) before employing the pPXF algorithm in our project. Subsequently, the kinematics are adjusted to accurately capture the stellar populations, which helps address potential issues caused by the Z-$\sigma_\star$ degeneracy. It is noteworthy that, in most instances, the inclusion of velocity dispersion results in a σ_T^2 ($\equiv \sigma_\star^2 + \sigma_{\rm inst}^2$) $> \sigma_{\rm MILES}^2$, enabling the utilisation of the MILES library without losing information.

The multiplicative polynomial is a mathematical function employed to correct flux calibration issues and other systematic factors present in the observed spectra. In this study we have established a multiplicative polynomial of 6.

Mathematically, any solution can be obtained from the fitting as long as it is a minimum of χ^2. Nevertheless, this solution linked to a particular instant in time may lack physical plausibility. Therefore, a regularisation factor is introduced to obtain an equally valid but smoother solution, one that is not associated with such sharp peaks of star formation, which are known not to exist in the universe as we know it. The regularisation determines a range of error within which possible solutions are considered, allowing for mathematically and physically correct results. For previous MEGARA data studies, regularisation factors of 5 have been used, as in the case of the work by Chamorro-Cazorla et al. (2023). Therefore, we have explored this range by analysing the factors of 0, 5, and 10.

4 Mock Spectral Models Analysis

In the MEGARA MR-G spectral range (4963 − 5443 Å), we miss the highly age-sensitive lines related to the Balmer series. As stated in Section 2, the primary challenge lies in determining the age associated with the galaxy's spectra in the absence of these lines. This entire section serves the purpose of providing robust methodological support for the stellar population results obtained in this study. Consequently, mock models of stellar populations have been developed using the MILES database (see Section 3.4). The SSP are then transformed into the observed characteristics presented by the MEGARA data to ensure that the values obtained through pPXF are accurate within a certain margin of error.

Within this section, our aim is to quantitatively determine the error and reliability margins of the stellar populations calculated with pPXF in the MEGARA spectral range. This will be done for the 0, 5 and 10 regularisations parameters and for signal-to-noise ratios of 10, 20, 40, and ∞. By doing so, we can establish the appropriate regularisation factor to be used in the pPXF fits for the galaxies and determine the minimum signal-to-noise requirement for each observed spectrum.

4.1 Mock spectra calculation

The mock spectral models consist of a collection of templates with varying ages and metallicity. Specifically, we have utilised the following ages: 1, 2, 3, 4, 6, 10, and 14 Gyr. As for the metallicity, we have chosen [M/H] = $-1.79, -1.26, -0.96, -0.25, 0.06, 0.26$, and 0.4, which allow us to cover values above, below, and close to solar metallicity. The age and metallicity range selected is intended to encompass the full parameter space and examine how each of them is affected when obtained through pPXF.

The MILES data, which are defined in the spectral range between 3525 − 7500 Å with a resolution of 2.50 Å and zero kinematics, do not align with the characteristics of the MEGARA data. Therefore, the initial step of this study involves generating mock spectral models by modifying certain parameters of the *base models* to match the characteristics of the MEGARA data. The following steps outline this process:

1. Firstly, an interpolation of the MILES templates has been performed to match the spectral sampling of the MEGARA data, which uses a pixel dispersion of 0.122 Å.

2. Secondly, the spectrum of the templates is shifted to account for a specific redshift. In this study, we have selected the mean redshift associated with the observed galaxies, which is z = 0.006786.

3. Next, the templates spectral range has been adjusted to cover 4960 − 5420 Å, corresponding to the MEGARA MR-G IFU mode data.

4. Finally, noise has been added to the models. While the real data are characterised by a specific signal-to-noise ratio per pixel that varies for each spectrum, it is not feasible to generate models for all these different S/N values, ranging from 2 to 80. Therefore, noise has been incorporated to produce spectra with S/N ratios of 10, 20, and 40.

4.2 Regularisation analysis

As explained in the pPXF section, regularisation is a crucial parameter in the calculation of stellar populations with this method. Therefore, we will determine the most suitable regularisation value for our sample. To achieve this, we will analyse the mock spectra using regularisation values of 0, 5, and 10 without adding signal-to-noise, representing the best-case scenario. Using pPXF, the selected mocks for this analysis

have been fit, resulting in separate outputs for age and metallicity.

Figure 5 displays the comparison between the known age and metallicity of the mock spectra and the best fit obtained after running pPXF.

This is done for different pPXF fitting schemes, varying the regularisation parameter. If the method were perfect and returned precisely the expected value, the points associated with each age and metallicity for different regularisations should align along the 1:1 line.

Additionally, we computed the error in the age and metallicity as the difference between the mesured value from the input value. This error is plotted against the input, allowing for a visual assessment of the quality of the pPXF fitting result.

Regarding age in Figure 5, a distinct trend is observed for young models compared to old ones: in the former case, the results are overestimated, while in the latter, an underestimation is obtained. Overall, metallicity is underestimated, yielding lower results than expected. This graph enables us to observe the differences found for the various regularisation factors.

Figure 6 shows the analysis of the statistical and systematic errors obtained using the mock spectra. The standard deviations and medians of the errors obtained with pPXF when fitting the mock data are calculated for the different regularisations.

Regarding the statistical errors for the age, it is observed that results with regularisation = 0 exhibit the greatest deviations, reaching 1.5 − 2.5 Gyr for large ages and a mean of ∼1.16 Gyr overall. Regularisations of 5 and 10 yield better and similar results, with smaller statistical errors: more concentrated data around a certain value. For metallicity, it is not as evident that regularisation is necessary, as the standard deviations return generally small values, all below 0.04. This implies that the data is more closely clustered around a specific value.

The statistical analysis concerning the median can reveal systematic errors that may occur for certain ages or metallicities. In terms of age, for values below 8 Gyr, the median is close to 0 for any regularisation, whereas for older ages, the median is higher and can even reach values up to 2 Gyr. In these cases, higher values are associated with regularisation = 0, while lower and closer values are observed for 5 and 10. Regarding metallicity, values close to zero are found across the entire range, except for metallicities of −0.96 and 0.04, where the median can exceed 0.15 for regularisation = 0.

Based on the comprehensive analysis conducted, it can be inferred that the regularisation factor plays a significant role in the MEGARA spectral range, and setting it to 0 is not suitable, as expected. This particular regularisation leads to higher data dispersion, resulting in erroneous outcomes in certain cases. It is worth noting that this effect is more pronounced when estimating the age of the stellar populations compared to determining their metallicity. This discrepancy is anticipated since age estimation is inherently more challenging in our study, while metallicity estimations are expected to be more robust, regardless of the chosen regularisation factor. Nonetheless, selecting between regularisation values of 5 and 10 presents a less straightforward decision. Evaluating both, the systematic error associated with the median and the standard deviation reveals slightly smaller values for the age with a regularisation factor of 5. Consequently, a marginal preference can be attributed to this one.

Additionally, selecting an excessively high regularisation value results in excessive smoothness, which can lead to poor fitting and an inability to capture important data features. Thus, following the principle of parsimony, the objective is to find a regularisation factor that minimizes unnecessary complexity while still maintaining a good representation of the fundamental characteristics of the stellar populations.

Taking all of the aforementioned discussion into consideration, it is concluded that a regularisation factor of 5 will be used for the MEGARA galaxies fit in this project. Furthermore, this is consistent with the results found in Chamorro-Cazorla et al. (2023).

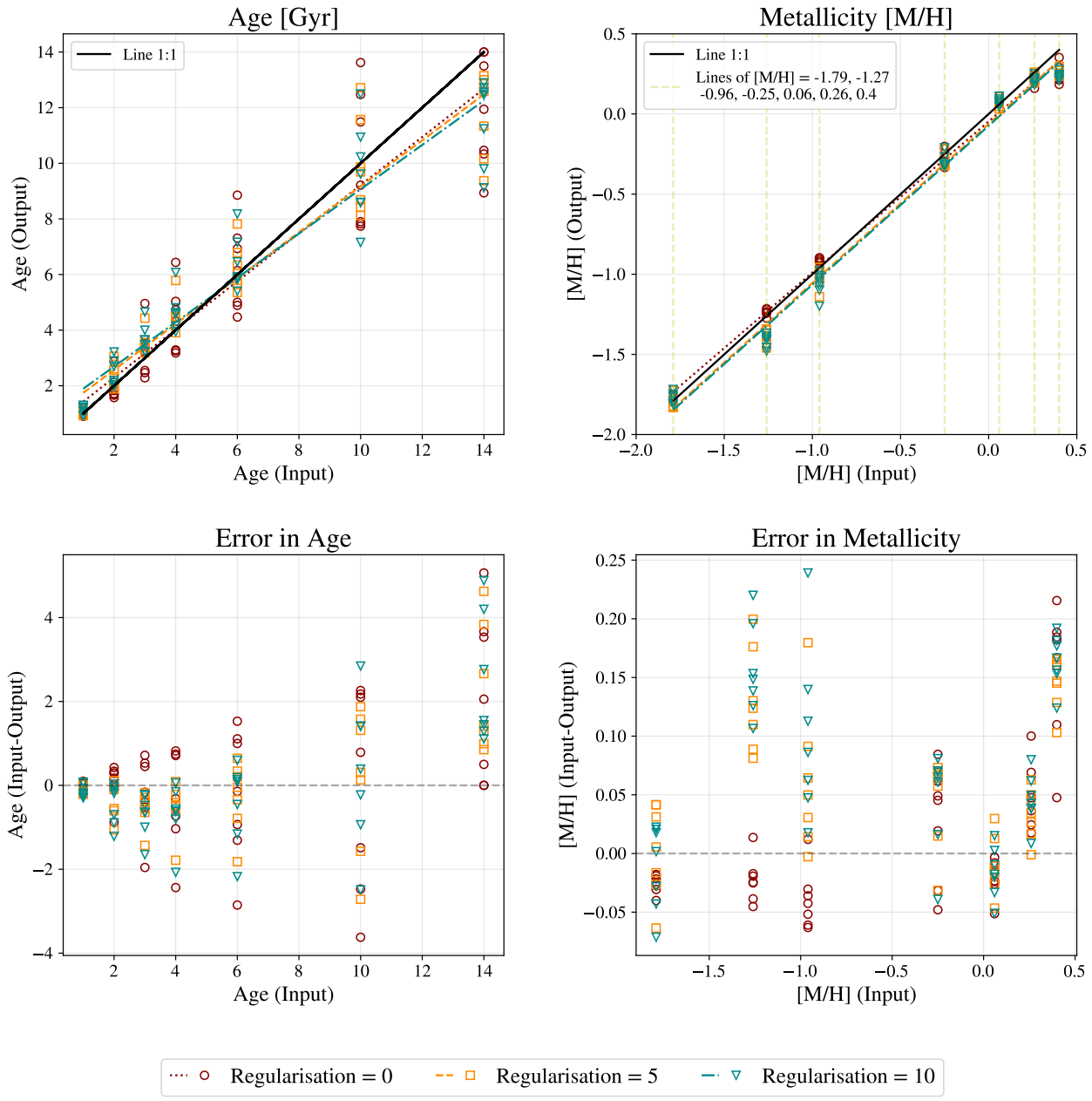

Figure 5: Performance of pPXF in recovering stellar population parameters through fitting of MEGARA-like mock spectra with different regularisation factors. The different linear fits to the pPXF results for regularisation = 0, 5, and 10 are presented in red dotted lines, in yellow dashed lines, and in dashed-dotted lines, respectively. With the same colours and shapes associated with dots, squares, and rectangles are presented the results of ages and metallicities for these regularisations. *Top panels*: The expected values of the models versus those obtained after pPXF fitting process are painted. The 1:1 line is shown in black to facilitate visual comparison. The left panel refers to the age in Gyr and the right panel shows the metallicity. *Bottom panels*: The values associated with the error (Input-Output) are shown, on the left is the age, and on the right is the metallicity. With a gray horizontal dash line, the 0 error, it represent the scenario where the output has the same value as the input.

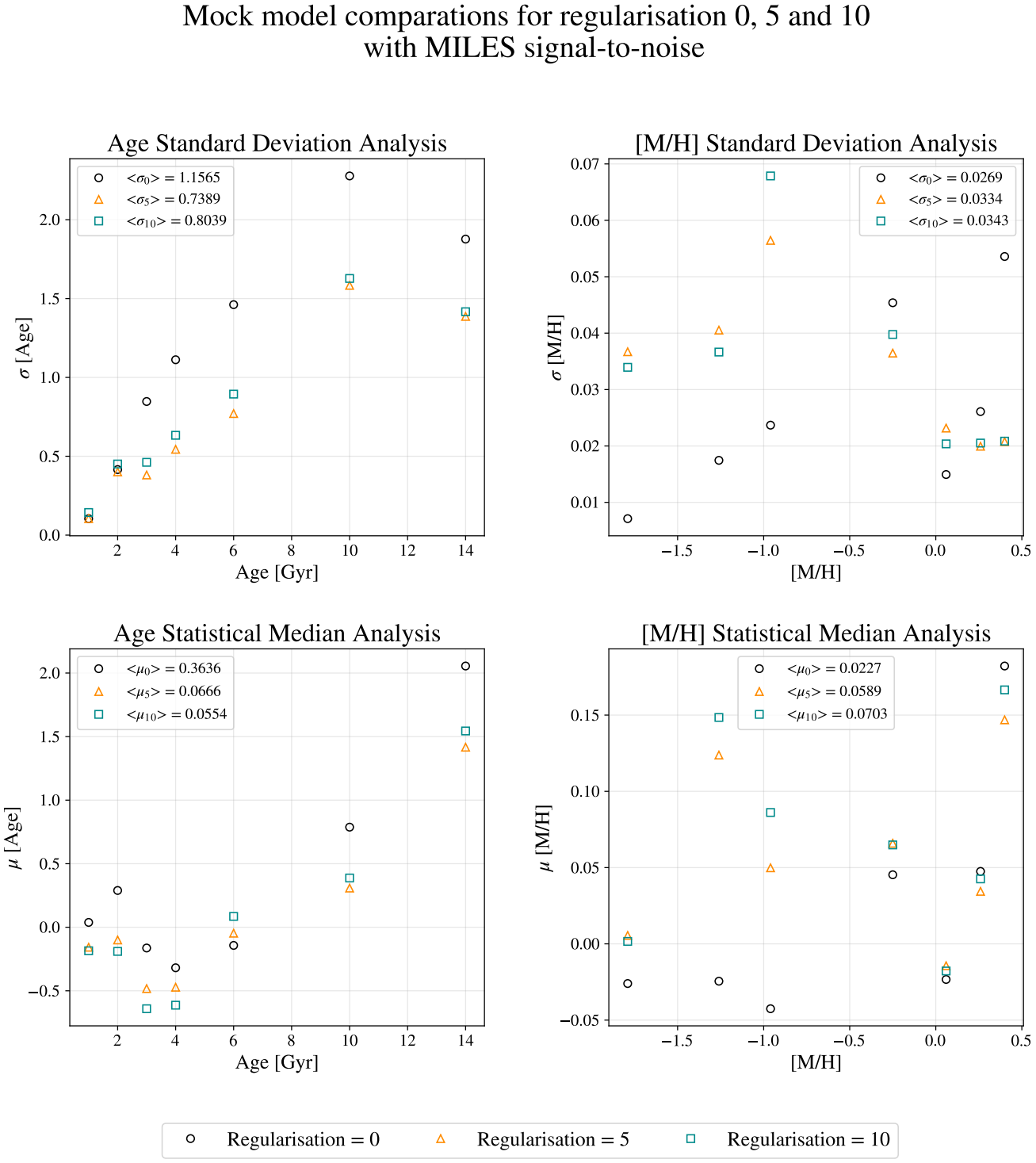

Figure 6: Mock model comparisons for different regularisation with MILES signal-to-noise. The standard deviation and median statistical errors (Input-Output) associated with the results obtained in the pPXF settings are shown in black dots, orange triangles, and blue squares for regularisations 0, 5, and 10 respectively. In the top panel the standard deviation, in the bottom panel the median, on the left the age, and on the right the metallicity.

4.3 Signal-to-noise analysis

The presence of noise in the spectra of the galaxies used for stellar population calculations is a crucial factor that determines the quality of the obtained results. To assess the reliability of our findings, we will determine the minimum signal-to-noise ratio at which the estimated age and metallicity become reliable. This will help establish the acceptable minimum S/N level for the data.

The *base models* from MILES are considered to have infinite S/N. The following study is conducted using mock spectra generated with different levels of noise, always for a regularisation factor of 5.

Figure 7 displays the results for S/N = 10. In this case, we observe a significant deviation from the 1:1 line in the linear fit to the age results, indicating a high dispersion. The associated error for ages below 7 Gyr typically varies within ±2 Gyr of the expected value. However, for older ages, the errors increase significantly, reaching up to 12 Gyr in some cases. Since the spectra for old populations tend to resemble each other considerably, determining their age accurately becomes more challenging. Which is further intensified by the low signal-to-noise ratio, leading to dramatic errors in some cases. Regarding metallicity, the results are slightly better, with lower dispersion and errors always within ±0.3 dex of the true value.

Figure 8 presents the results for S/N = 20, showing a considerable improvement. The linear fit of the pPXF output data align more closely with the 1:1 line for the stellar populations properties, although there is still high dispersion for older ages. Regarding age errors, they worsen beyond 10 Gyr, reaching inaccuracies of up to ±6 Gyr. It is worth noting that errors for 14 Gyr spectra are always positive since there are no models for older ages, making it impossible for the fit to surpass that value. On the other side, the maximum errors for metallicity are ±0.2 across the considered range.

Figure 9 displays the mock spectral analysis for S/N = 40, showing results more similar to those without noise (see Figure 5). The age errors remain generally low for most of the range (< ±2 Gyr), except for ages of 14 Gyr, where errors can reach up to 6 Gyr. Metallicity appears to be well-constrained, although the results are consistently underestimated.

A statistical analysis of the results, shown in Figure 10, reveals that both age and metallicity exhibit higher standard deviation errors for lower S/N and tend to approach zero as S/N tends to infinity, as expected. Additionally, the standard deviation for age is consistently higher compared to metallicity.

The median shows a negative systematic error for younger ages, indicating an overestimation of the results. Conversely, for older ages, a positive systematic error is observed, with errors reaching up to 3 Gyr. This means that the results may be contaminated with younger ages for older galaxies. Regarding metallicity, it is more complex to consider the median as a systematic error since it only works when the dispersion in errors is not substantial. As observed in the panels on the right-hand side of the bottom panel in Figures 7, 8, and 9, the metallicity values do not show a clear trend. At a fixed metallicity, the dispersion of the points in the output-input differences is so high that it spans a wide dynamic range, resulting in points both below and above zero. When taking the median, values close to zero are obtained, giving the illusion of no systematic errors. That is why the mean value appears closer to 0 for worse signal-to-noise ratios, not because the error is smaller, but because as the S/N decreases, it becomes more challenging to determine the error due to increased dispersion. However, this indicates that a systematic error cannot be established, rather than implying its absence.

Generally, errors are larger for older ages, which becomes evident due to the similarity acquired by the spectra when ages are around $10 - 14$ Gyr, making it more difficult to accurately fit the spectra in this region. Figure 11 provides an illustrative example of three single stellar populations (SSPs) at ages 10, 12, and 14 Gyr, highlighting the challenges mentioned.

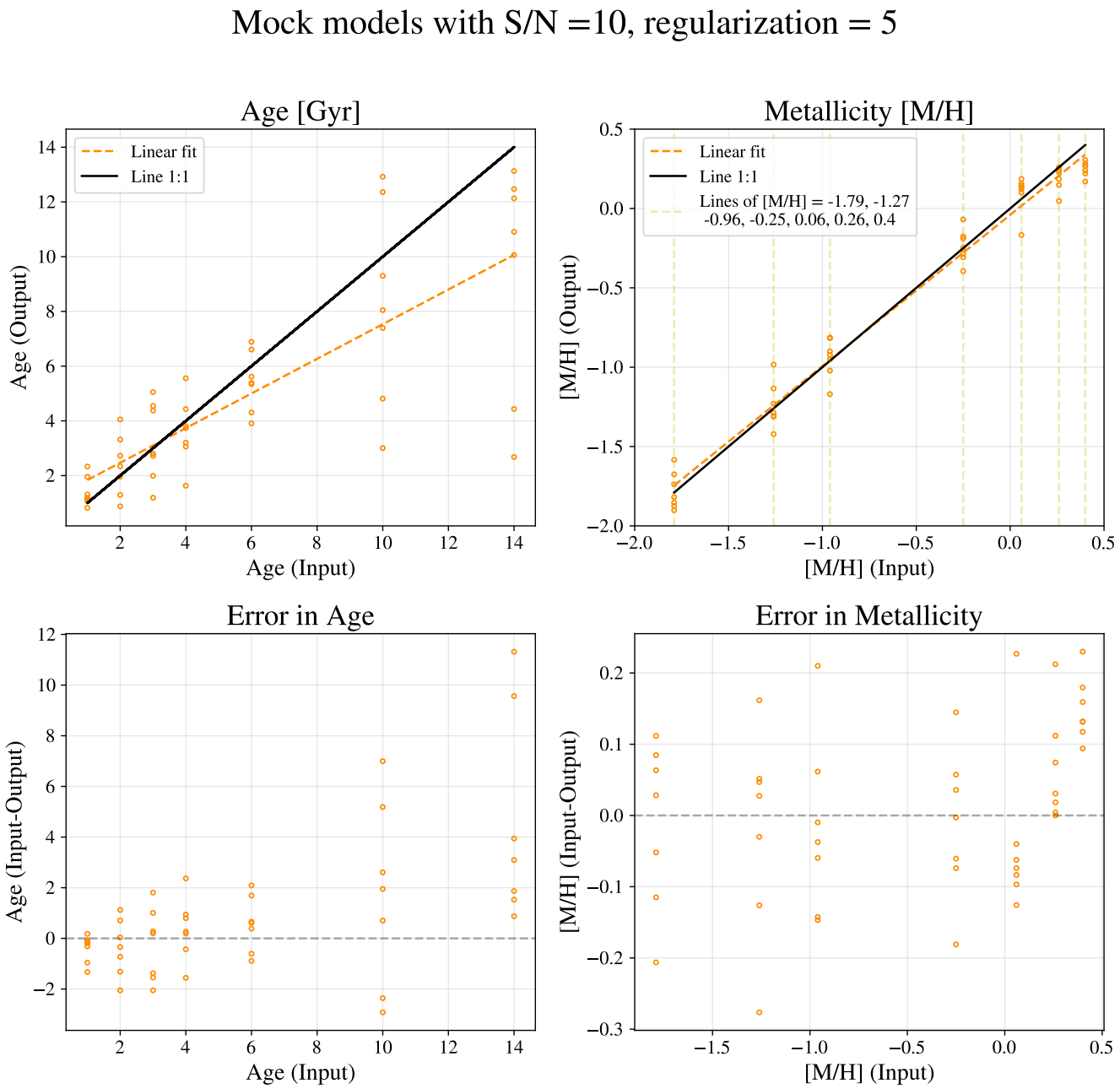

Figure 7: Performance of pPXF in recovering stellar population parameters through fitting of MEGARA-like mock spectra with S/N=10 and a regularisation factor of 5. *Top panels*: Linear fits of pPXF results for ages and metallicities are presented in yellow dashed lines. In yellow circles the expected values of the models are plotted against those obtained after pPXF fitting process. The 1:1 line is shown in black to facilitate visual comparison. The left panel represents the age in Gyr and the right panel shows the metallicity. *Bottom panels*: The values associated with the error (Input-Output) of the expected value minus the obtained one are shown in yellow circles, on the left is the age, and on the right is the metallicity. With a gray horizontal dash line, the 0 error,it represent the scenario where the output has the same value as the input.

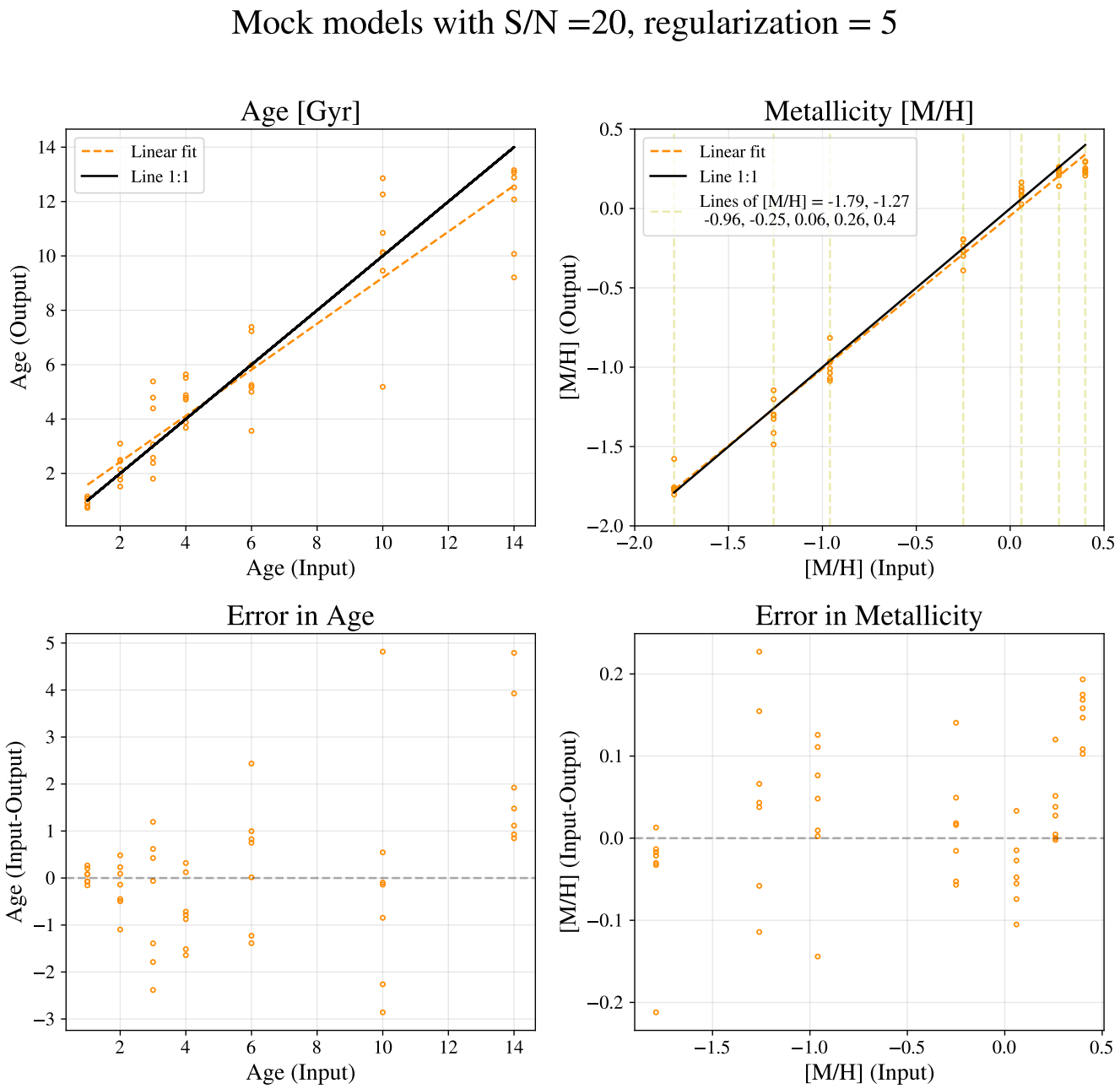

Figure 8: Performance of pPXF in recovering stellar population parameters through fitting of MEGARA-like mock spectra with S/N=20 and a regularisation factor of 5. *Top panels*: Linear fits of pPXF results for ages and metallicities are presented in yellow dashed lines. In yellow circles the expected values of the models are plotted against those obtained after pPXF fitting process. The 1:1 line is shown in black to facilitate visual comparison. The left panel represents the age in Gyr and the right panel shows the metallicity. *Bottom panels*: The values associated with the error (Input-Output) of the expected value minus the obtained one are shown in yellow circles, on the left is the age, and on the right is the metallicity. With a gray horizontal dash line, the 0 error, it represent the scenario where the output has the same value as the input.

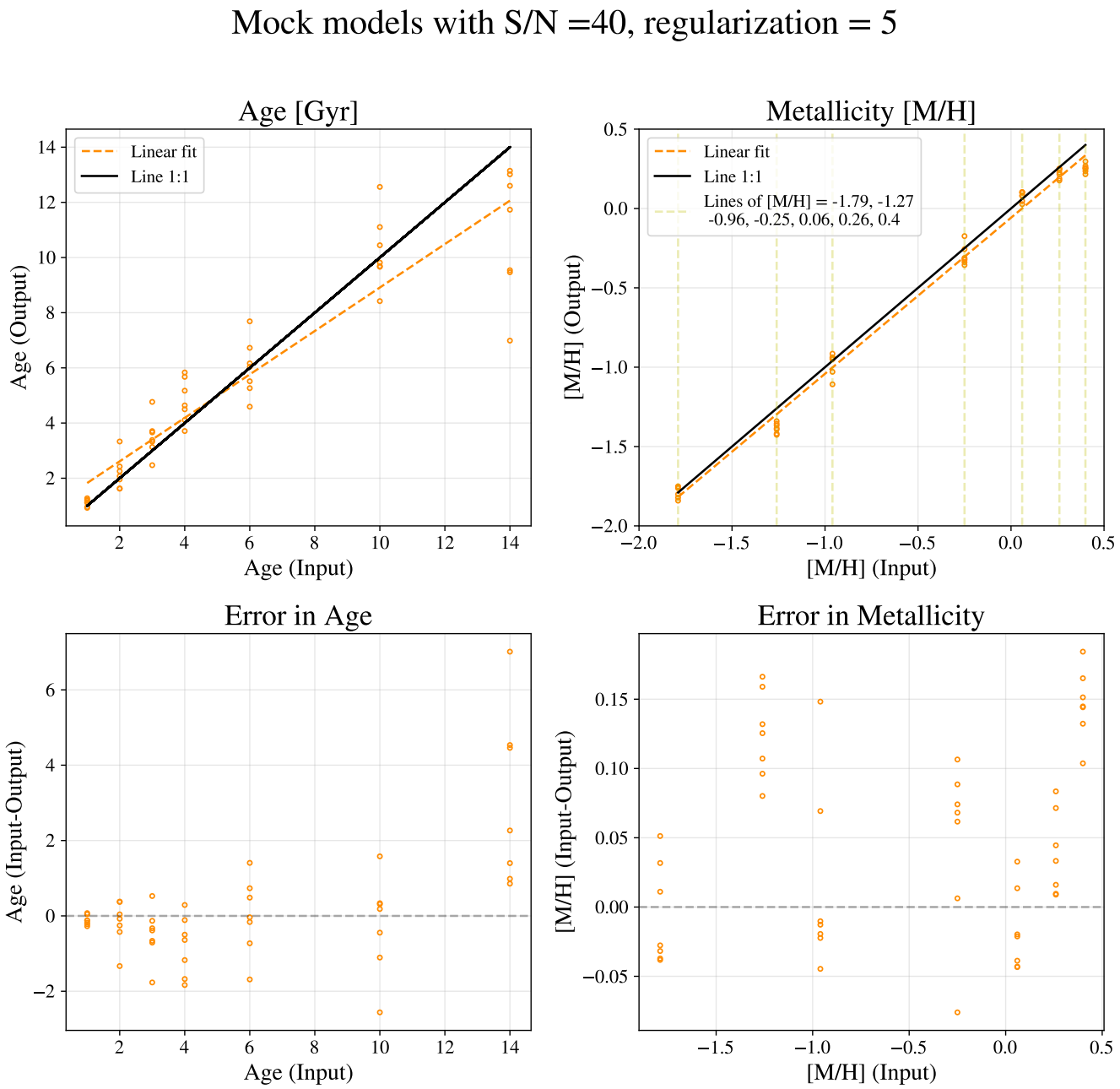

Figure 9: Performance of pPXF in recovering stellar population parameters through fitting of MEGARA-like mock spectra with S/N=40 and a regularisation factor of 5. *Top panels*: Linear fits of pPXF results for ages and metallicities are presented in yellow dashed lines. In yellow circles the expected values of the models are plotted against those obtained after pPXF fitting process. The 1:1 line is shown in black to facilitate visual comparison. The left panel represents the age in Gyr and the right panel shows the metallicity. *Bottom panels*: The values associated with the error (Input-Output) of the expected value minus the obtained one are shown in yellow circles, on the left is the age, and on the right is the metallicity. With a gray horizontal dash line, the 0 error, it represent the scenario where the output has the same value as the input.

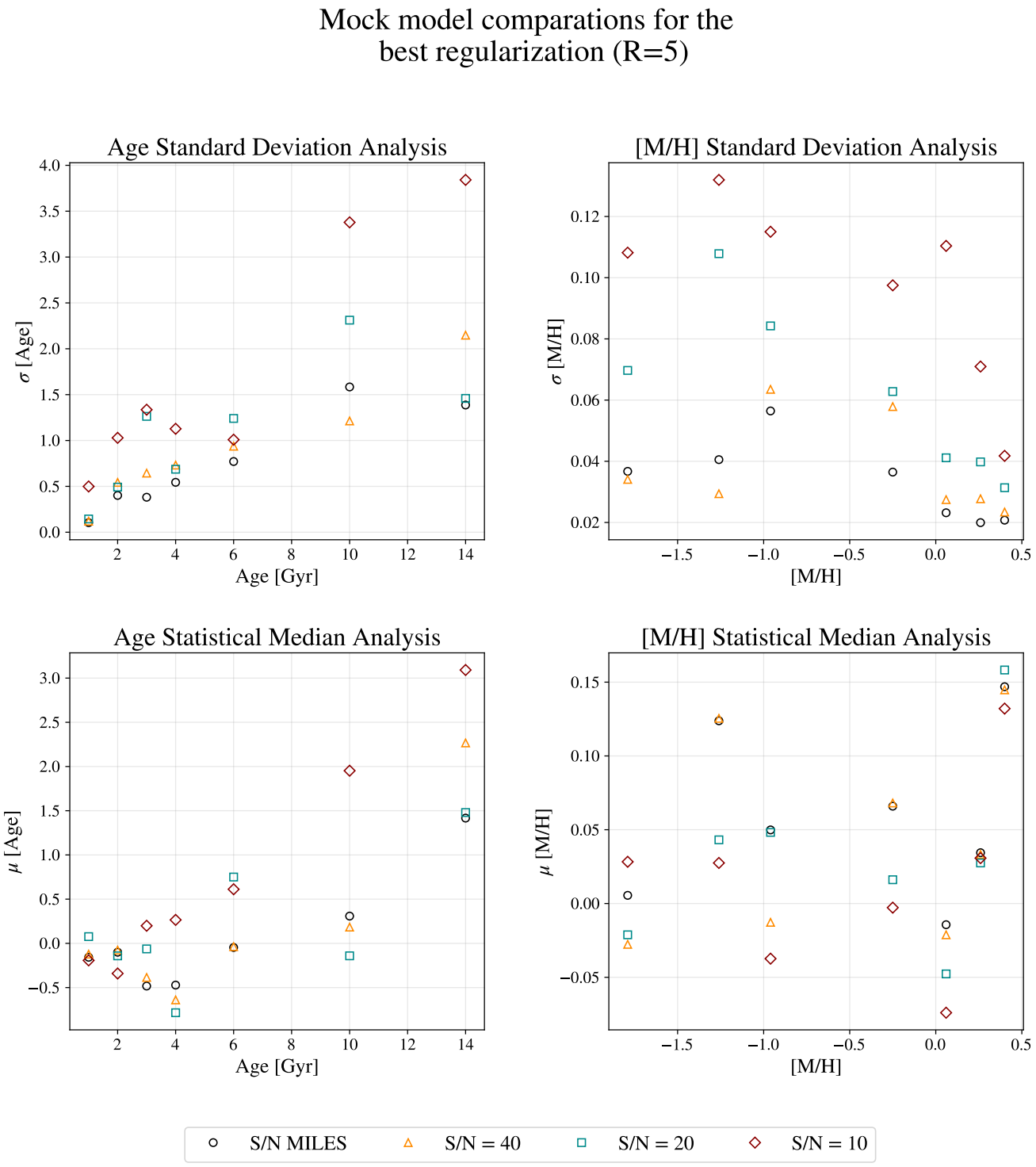

Figure 10: Mock model comparisons for the best regularisation (R = 5) with different S/N. The standard deviation and median statistical errors (Input-Output) associated with the results obtained in the pPXF fit for each signal-to-noise are plotted in black dots, orange triangles, blue squares, and red pentagons for S/N = ∞, 40, 20, 10 respectively. In the upper panel the standard deviation, in the lower panel the median, on the left the age, and on the right the metallicity.

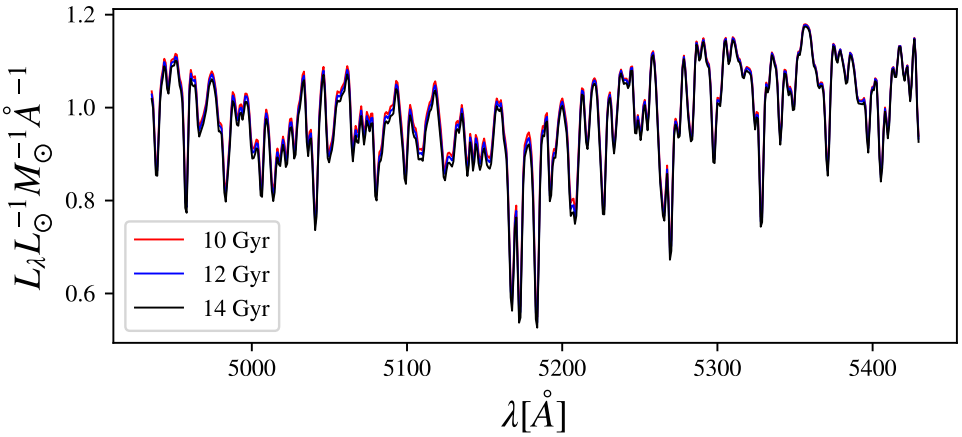

Figure 11: Base MILES models in the MEGARA spectral range for a metallicity of [M/H] = 0.06 and ages of 10, 12 & 14 Gyr in red, blue and black, respectively.

In conclusion, higher S/N values lead to more reliable results, and they are excellent starting from S/N = 40. For lower S/N values (30 − 20), although the results are less certain, consistent values can still be obtained. It is for S/N ∼ 10 that the results become less accurate, with significant deviation in the values returned by pPXF, making it impossible to determine systematic errors.

Based on this analysis, we conclude that for our study, we will consider only those galaxy spectra with an S/N > 15. This ensures that, in general, the results will prevent inconsistencies in the calculation of stellar populations.

4.4 Mock models conclusions

As a conclusion to this chapter, it can be inferred that one of the main objectives of this study has been successfully achieved: the determination of the age in the spectra covering the wavelength range of 4965−5445 Å.

The minimum S/N established for our data is 15, which means discarding the galaxies NGC 1090, NGC 3756, NGC 4062, UGC 4375, NGC 3614, and NGC 5320.

Furthermore, it has been possible to establish the applied error for the results. This is displayed in Table 2, where the average errors have been defined for each of the considered age and metallicity ranges in the case of S/N = 20 & 10. Such errors are an upperlimit in most cases as the majority of the spaxels of our MEGARA data have S/N well above 20, reaching even S/N > 70. However, in order to be consistently, we have always consider in this thesis the errors associated with S/N = 10, which are in bold in Table 2.

Table 2: Errors associated with the various age and metallicities ranges for the MEGARA data. They have been derived from the analysis of mock models under the condition of S/N=10 & 20.

	Range	Statistical error		Systematic error		Total error	
S/N		10	20	10	20	10	20
Age [Gyr]	0 − 4	± 0.99	± 0.65	− 0.01	− 0.23	± **1.00**	± 0.42
	4 − 7	± 3.40	± 2.31	+1.95	± 0.14	± **5.33**	± 2.17
	7 − 12	± 3.61	± 1.89	+ 2.52	± 0.67	± **6.13**	± 2.55
Metallicity	−2 − 0.4	± 0.10	± 0.06	-	-	± **0.10**	± 0.06

5 Results and discussion

5.1 Stellar population maps

In this section, we will analyse the results obtained for the stellar population analysis conducted for the BEARD survey subsample consisting of 21 galaxies. For each galaxy we have produced two maps, one indicating the age and the other showing the metallicity of these celestial objects. Figures 12(a), 13(a) , 14(a) display the maps for three specific galaxies, NGC 5962, NGC 4405, and NGC 1087, while the remaining maps can be found in Appendix A. Additionally, Figures 12(b), 13(b), and 14(b) showcase the best signal-to-noise spaxel fits and the corresponding age-metallicity plane for that spaxel. In Figure 15, the histograms associated with the age and metallicity of the spaxels in the bulge of the galaxies are displayed. These histograms are presented to enable a more in-depth analysis of the central region of the galaxies. These particular galaxies were selected as representative examples of this study due to their distinctive characteristics (what we will see in their age-metallicity planes and stellar population maps), which can serve as a reference for the rest of the sample. This analysis has been conducted for all the galaxies under investigation.

5.1.1 NGC 5962

NGC 5962 is observed as a pure bulgeless galaxy situated at a distance of approximately 30 Mpc (Tully et al., 2008). The bulge radius has been determined to be 1″, as depicted in black solid line in the maps shown in Figure 12(a). The galaxy exhibits a significantly high signal-to-noise ratio, allowing for the recovery of an expansive field of view of almost 12″ with S/N> 15.

The structure of NGC 5962 is clearly discernible. In the central region, there exists an area of older stellar populations, although it does not appear as an excessively aged "bulge". The mean mass weighed age of this region is estimated to be around 3.5 Gyr, with a higher metallicity compared to its immediate surroundings, at [M/H]= 0.04. As we can observe in the top panel of Figure 15: all spaxels consistently display an age below 4 Gyr and a metallicity below 0.1 dex. This distinctive region extends between −1″.2 and 0″.8 in the x-axis of the field of view. Moreover, a younger stellar population ring (∼1 Gyr) is evident, exhibiting a metallicity range of [M/H]= −0.4 to 0.2 dex (inside out), with a notable deep gap.

Regarding its fitting (see Figure 12(b)), it has been successfully achieved with generally minimal errors, primarily due to the high signal-to-noise ratio in the bulge region (> 70, as shown in Figure 3). The age estimation returns errors of approximately ±1 Gyr, owing to the relatively young age of the population (within the $[0-4]$ Gyr range). As for metallicity, the errors amount to ±0.1 dex (see Table 2).

The age-metallicity plane of the central spaxel of NGC 5962 demonstrates a significant and prolonged main starburst that extends from 9 Gyr to 2 Gyr ago, with metallicity confined within a relatively narrow range centred in 0.04. Additionally, there appears to be a minor, younger starburst with lower metallicity, possibly indicating some gas accretion from outside the bulge. However, this contribution remains negligible compared to the primary starburst.

5.1.2 NGC 4405

NGC 4405 is observed as a galaxy located at a distance of approximately 16.5 Mpc (Cappellari et al., 2011). According to the photometric decomposition conducted by Zarattini et al. (in preparation), it has a bulge effective radius of 1″.59. Generally, this galaxy exhibits a lower signal-to-noise ratio compared to NGC 5962. Nevertheless, it was still possible to obtain stellar population results for the entire bulge region. The left map in Figure 13(a) illustrates a central bulge that appears younger than its immediate surroundings, although the gradient following this trend is not clearly discernible due to

signal limitations in the data. As a whole, the bulge exhibits an age of approximately $2 - 2.5$ Gyr (as we can see in the medium panel of Figure 15), which corresponds to a relatively low, but higher-than-average, metallicity compared to the surrounding environment, with [M/H] values ranging from -0.4 to -0.2 dex (see right panel of Figure 13(a)). Furthermore, the metallicity indicates that the majority of bulge spaxels have a value around -0.25 dex.

Regarding the fitting process (see Figure 13(b)), it is evident that it has been successfully accomplished, albeit with some lines not completely aligning with the highest flux peaks. It is important to note that in this case, the signal-to-noise ratio is lower, and therefore, the fit may not perfectly replicate the spectrum. However, these discrepancies remain within the error margins discussed in the Table 2.

The age-metallicity plane of the center spaxel of NGC 4405 is somewhat more intricate than the previous case. It demonstrates an initial extended starburst approximately 6 Gyr ago, which lasted from 7.5 to 1.5 Gyr ago, with a metallicity around -0.8. Subsequently, a more intense and recent starburst occurred with a higher metallicity of 0.05. This scenario is interpreted as a series of events wherein a first generation of stars originated from the existing gas within the galaxy, followed by a second generation that formed from gas enriched by the metals expelled by the death of the more massive stars of that first generation.

5.1.3 NGC 1087

NGC 1087 is situated at an approximate distance of 21.8 Mpc (Mould et al., 2000). According to the photometric decomposition by Zarattini et al. (in preparation), it has an effective radius for the bulge of $1''.74$. However, recent studies by BEARD suggest that it is a pure bulgeless galaxy, and the region previously considered as a bulge is actually a region of ongoing star formation (del Socorro-Prieto, (2023, Master thesis)).

In the left map of Figure 14(a), it can be observed that, overall, the entire region of the galaxy where stellar population calculations have been performed (bulge and surroundings) exhibits predominantly very young stellar populations, barely exceeding 3 Gyr. We are in a scenario of very recent star formation, which is further supported by the age errors of approximately ± 1 Gyr for such young ages found in this system. The spaxels that compound the "bulge", are always below the 2 Gyr, the most part of them around 1 Gyr as we can see in the bottom panel of Figure 15. In the right map of Figure 14(a), associated with metallicity, distinct blobs of different [M/H] values can be distinguished. Here, specific structures in a wide dynamic range of metallicities can be determined, ranging from -1.6 to -0.2, always lower than solar metallicity. The spaxels in the "bulge" maintain this trend, as seen in the bottom panel histograms of Figure 15, due to the aforementioned blobs. These structures could indicate recent gas inflow that may come from external origin.

Figure 14(b) illustrates the fitting of the spaxel with the highest signal-to-noise ratio (S/N = 50), where significant spectral emission can be observed, in agreement with a scenario of star formation. However, the spectrum has not been perfectly fitted due to the distortion caused by the strong emission (even if the line is in the fit), which also exhibits residuals due to the wings of the Gaussian fit to the line. Regarding its age-metallicity plane, we observe two main starburst events occurring approximately 0.55 Gyr and 0.20 Gyr ago, which are relatively close in time, suggesting that they may be consequences of the same event.

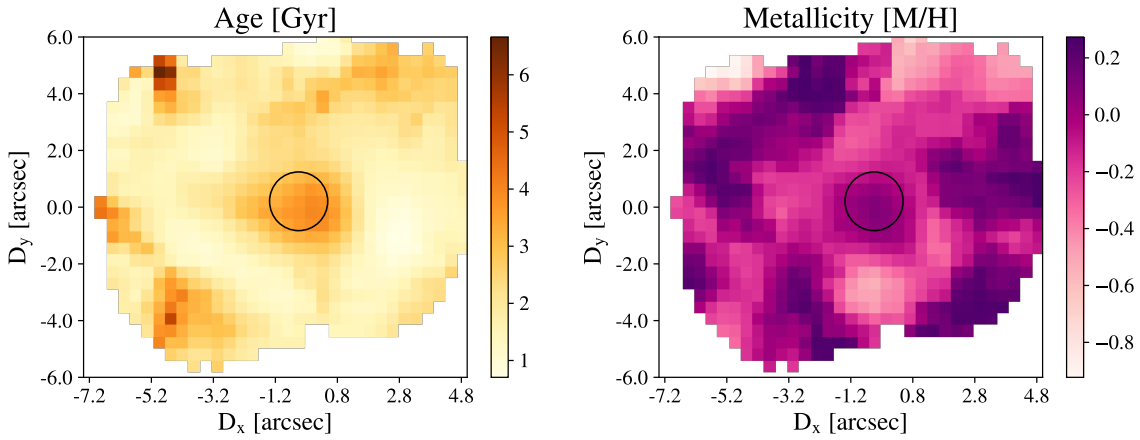

(a)

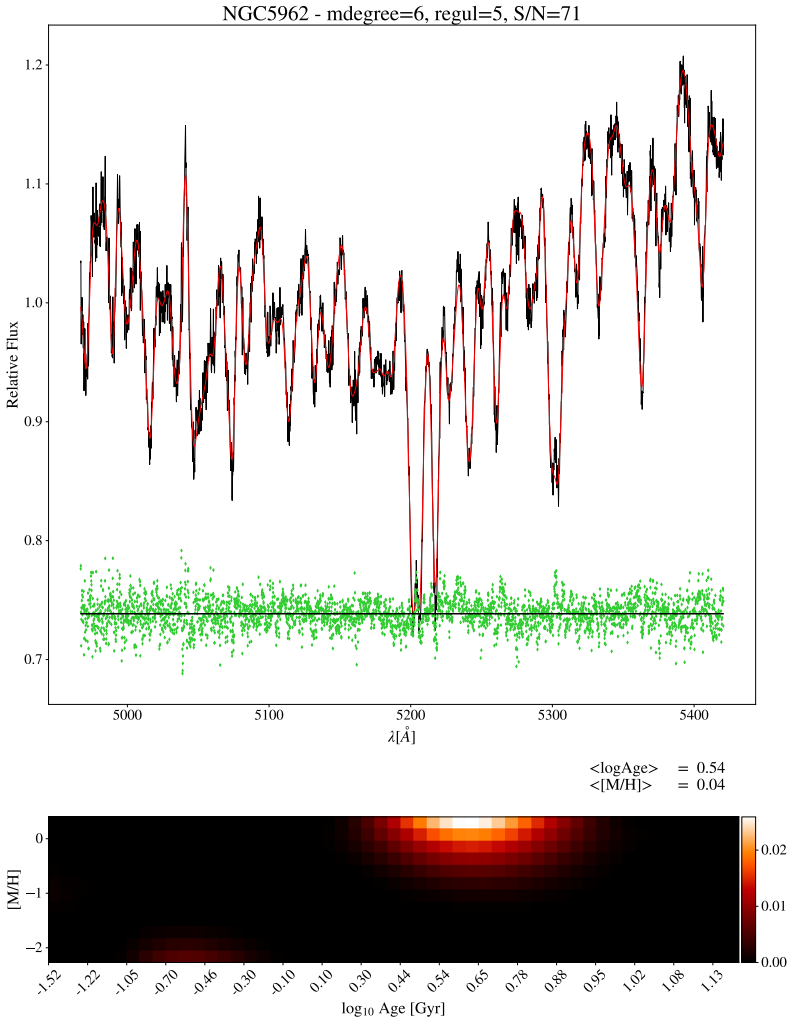

(b)

Figure 12: ***(a)***: Stellar population maps for NGC 5962. On the left, the age map, and on the right, the metallicity map. *1″ = 145.5 pc.* ***(b)*** *Top panel*: Fit performed with pPXF for the spaxel with the highest signal-to-noise ratio in the galaxy (S/N = 71). The black line is the spectrum of the galaxy, the red line is the best fit obtained by pPXF and the green dots are the residuals, with their median represented as a black horizontal line. ***(b)*** *Bottom panel*: Shows the weights of all the used templates, it represents the age-metallicity plane.

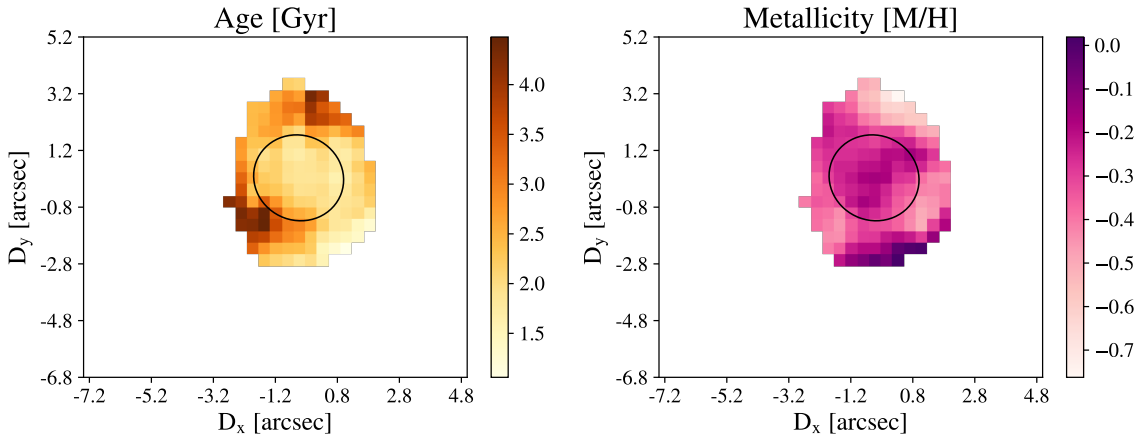

(a)

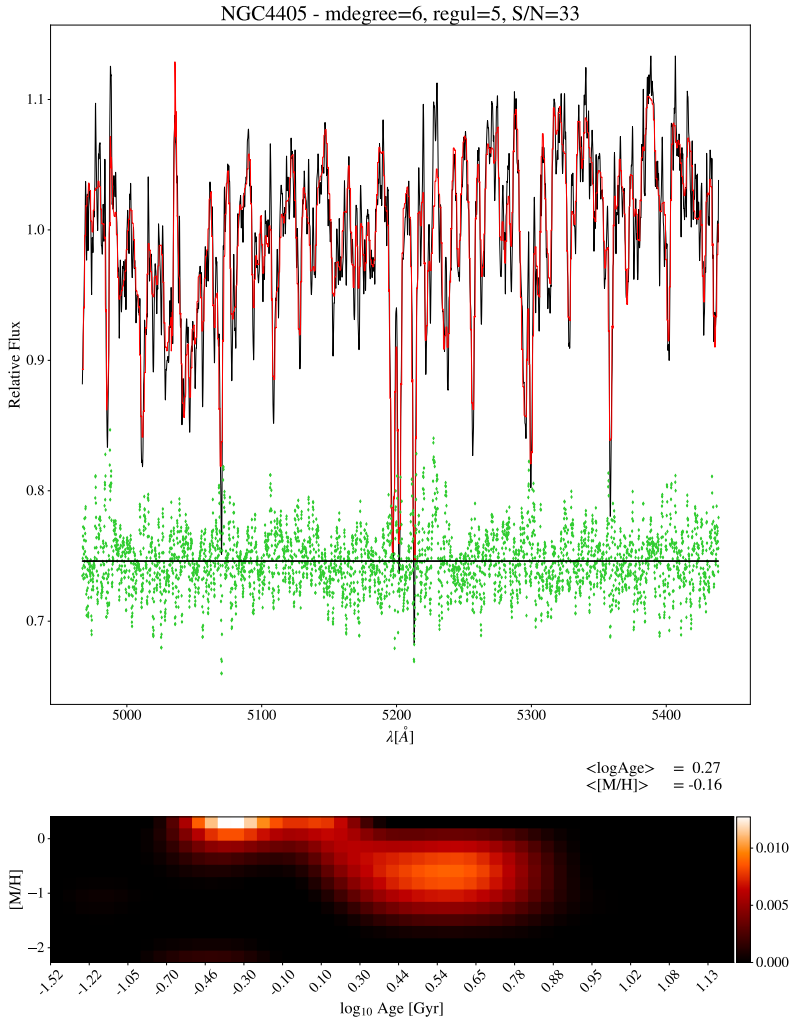

(b)

Figure 13: ***(a)***: Stellar population maps for NGC 4405. On the left, the age map, and on the right, the metallicity map. *1″ = 80.0 pc*. ***(b)*** *Top panel*: Fit performed with pPXF for the spaxel with the highest signal-to-noise ratio in the galaxy (S/N = 33). The black line is the spectrum of the galaxy, the red line is the best fit obtained by pPXF and the green dots are the residuals, with their median represented as a black horizontal line. ***(b)*** *Bottom panel*: Shows the weights of all the used templates, it represents the age-metallicity plane.

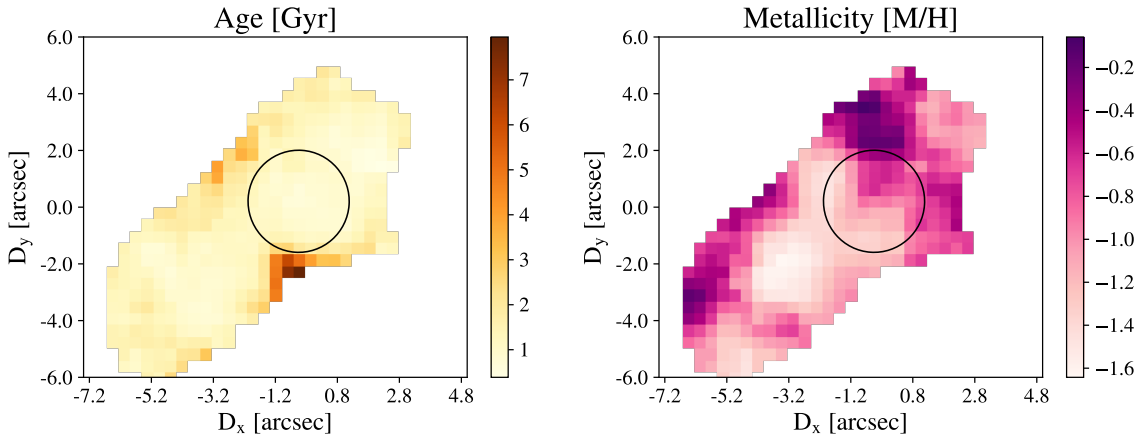

(a)

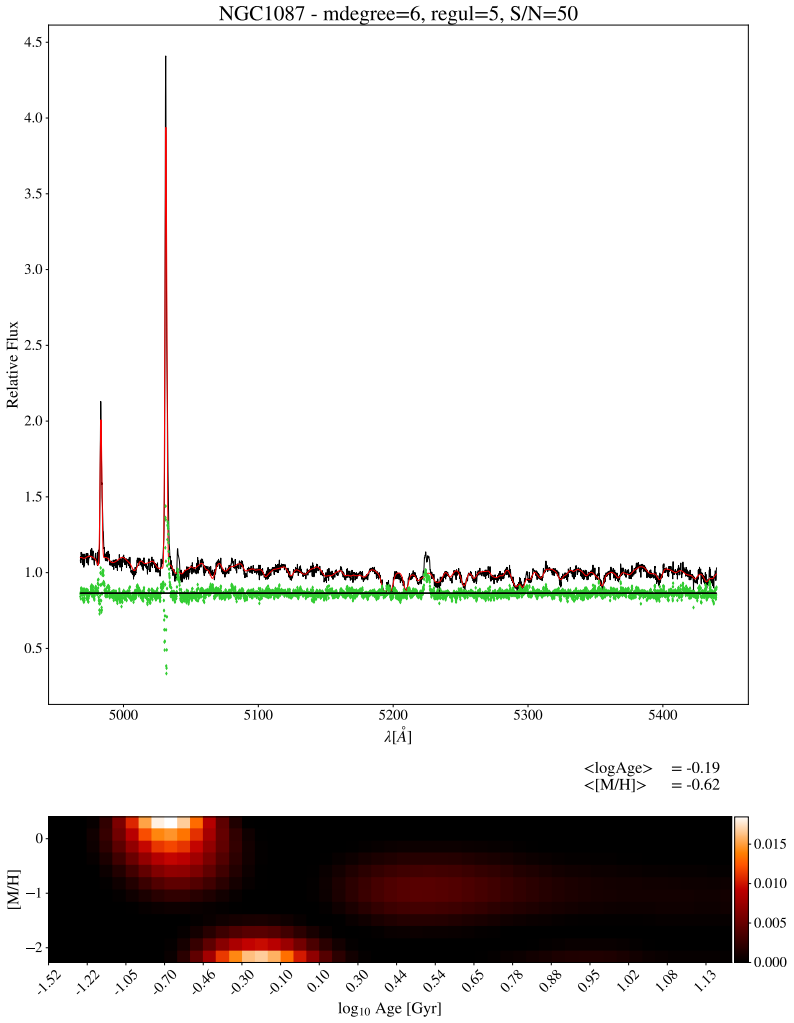

(b)

Figure 14: ***(a)***: Stellar population maps for NGC 1087. On the left, the age map, and on the right, the metallicity map. *1″ = 105.7 pc.* ***(b)*** *Top panel*: Fit performed with pPXF for the spaxel with the highest signal-to-noise ratio in the galaxy (S/N = 50). The black line is the spectrum of the galaxy, the red line is the best fit obtained by pPXF and the green dots are the residuals, with their median represented as a black horizontal line. ***(b)*** *Bottom panel*: Shows the weights of all the used templates, it represents the age-metallicity plane.

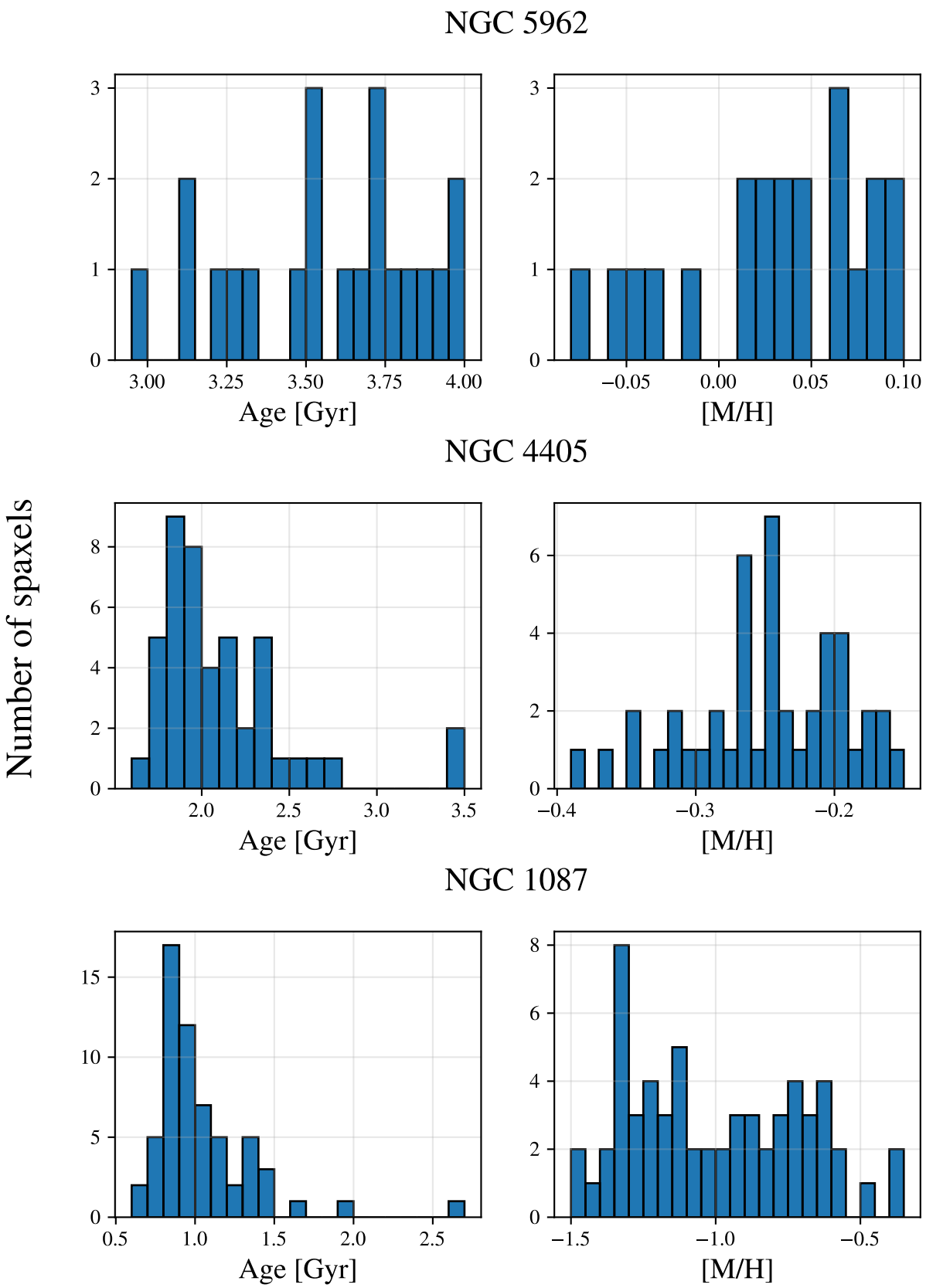

Figure 15: Histograms associated with the spaxels contained within the effective radius of each of the bulges studied in Section 5.1. From top to bottom: NGC 5962, NGC 4405, NGC 1087; on the left, the age (bins = 0.05, 0.1, 0.1 Gyr respectively), and on the right, the metallicity (bins = 0.01, 0.01, 0.05 dex respectively).

5.2 Bulge formation scenario

In this section, the aim is to better understand the bulge formation scenario in the BEARD sample by comparing them with the results of stellar population of literature.

The data used for this comparison is the CALIFA sample presented in Méndez-Abreu et al. (2021), which examines 129 unbarred galaxies from CALIFA DR3 covering a wide range of stellar masses and Hubble types (Sánchez et al., 2016a). These galaxies have been spectrophotometrically decomposed into disc and bulge components using the `c2d` code (Méndez-Abreu et al., 2019). Among them, there are 58 galaxies classified as bulge-to-disc, 40 bulge-to-disc with a break, and 31 early-type galaxies. Stellar populations for these galaxies have been derived in de Lorenzo-Cáceres et al. (in preparation) using the PIPE3D pipeline developed by Sánchez et al. (2016b).

Figure 16 displays the results of stellar population analysis obtained from CALIFA and the results obtained in this study. For each BEARD galaxy we are plotting all spaxels within the bulge radius (we use always the radius derived in Zarattini et al. (in preparation)), it implies one only mass value but a range of ages and metallicities. Blue circles represent CALIFA data, yellow circles represent MEGARA data, and red triangles represent the central spaxel of each galaxy in our sample, corresponding to the central point of the effective radius of the bulge ellipse (the highest S/N spaxel). In the top panel, the analysis of age as a function of bulge mass for different systems is divided into three regions. Each age region is associated with a specific error indicated as $\sigma_{\rm age}$. We use this way of showing the typical errors on our measurements because the same galaxy may exhibit spaxels with different errors as stated in Table 2. In the bottom panel, a similar analysis is presented for metallicity, with the error also specified ($\sigma_{\rm [M/H]}$), but in this case, it is the same for all values of [M/H], as explained in Section 4.4.

The CALIFA data analysed in de Lorenzo-Cáceres et al. (in preparation) show that as the bulge mass decreases, the range of ages in their stellar populations increases, while more massive systems tend to be older and more metal-rich. This trend results in a triangular-shaped plot, which is also discernible (although more subtly) for metallicity. Lower metallicities correspond to less massive bulges. de Lorenzo-Cáceres et al. (in preparation) also observe this trend in relation to the whole galaxy mass. When comparing these results with our data, the first noticeable result is that, in general, the MEGARA bulges are much younger than these present in the CALIFA sample. A similar trend is observed for metallicity, but in this case BEARD bulges are generally more metal-rich than these in CALIFA. It is crucial to take into consideration that the masses of the BEARD galaxies are in the same regime as the masses of the CALIFA galaxies, albeit hosting significantly more diminutive bulges.

Our interest lies in understanding what sets these bulges apart, as they challenge the hierarchical formation model. From this study, we infer that our bulges are forming stars most likely from disc material, rather than being structures formed since high redshift, as could be the case in the CALIFA sample. This behaviour suggests the occurrence of a secular evolution associated with the evolution of the disc over time, ruling out a formation scenario through mergers.

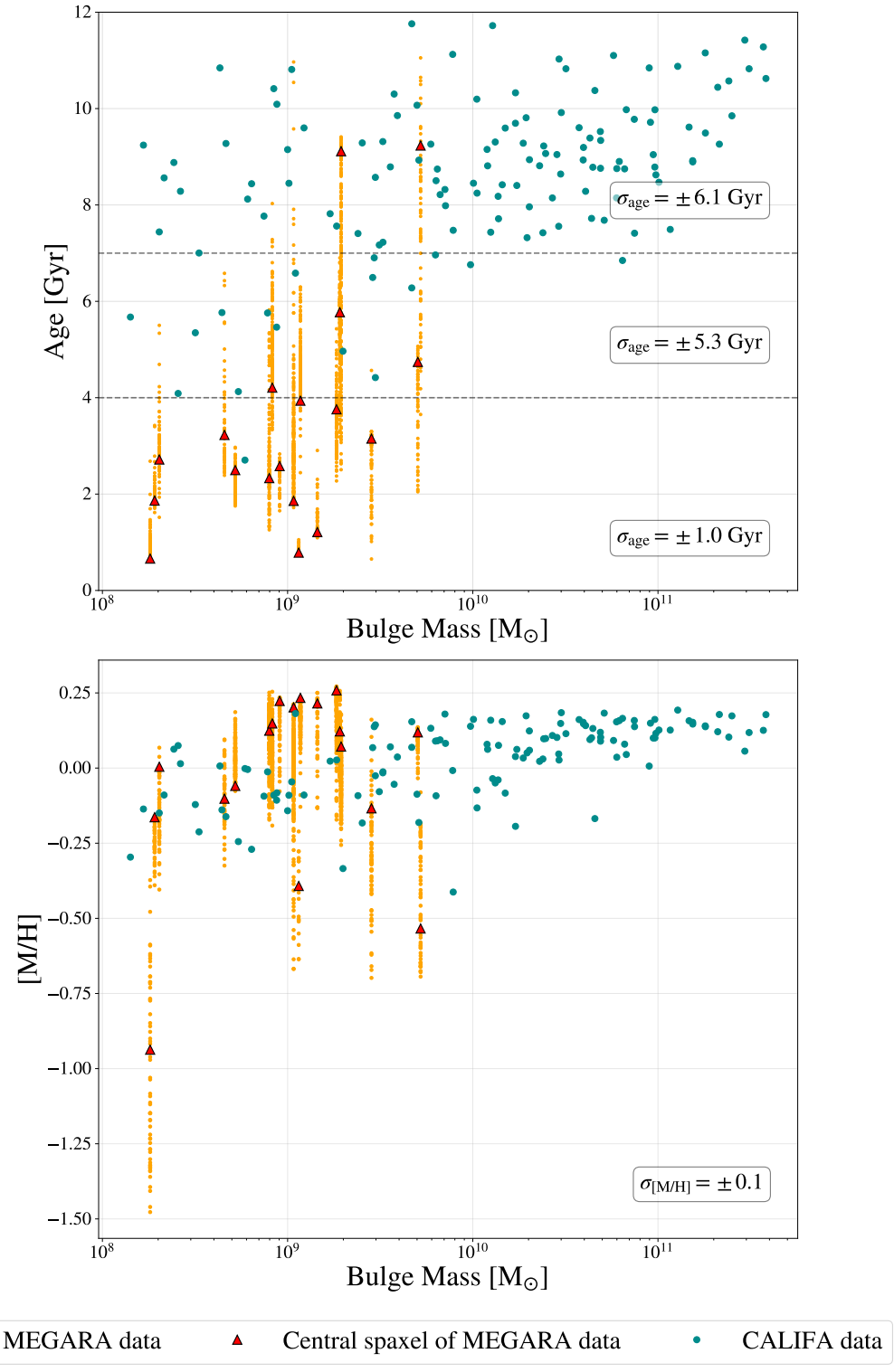

Figure 16: MEGARA and CALIFA galaxies bulge comparison. In yellow circles, the results associated with MEGARA data for each individual spaxel, in red triangles, the results associated with the central spaxel of the BEARD bulges, and in blue circles, the results from CALIFA analysed in de Lorenzo-Cáceres et al. (in preparation). *Top panel*: Age vs bulge mass (see Table 1), with errors indicated on the right side of the panel for each age range, considering Table 2 for S/N=10, thus including upper limits in the errors. *Bottom panel*: Metallicity vs bulge mass. On the right side, the error found for metallicity derived from the analysis in Section 4.

6 Conclusions

The spectroscopic analysis of BEARD bulgeless galaxies, carried out with MEGARA, has allowed us to achieve the main objective of this work: to demonstrate the feasibility obtaining stellar populations in data that do not contain lines sensitive to age. Consequently, the main characteristics of the stellar populations found in the central regions of our data have been reliably determined. This has been accomplished thanks to various aspects studied in this work. Therefore, based on the MEGARA results, we have reached the following conclusions:

i. The robustness of the code has been confirmed through the mock spectra models, demonstrating the ability to accurately obtain stellar populations despite the absence of lines such as Hβ.

ii. Errors have been obtained for ages and metallicities. These errors are $\pm$1 Gyr for the 0$-$4 Gyr range, $\pm$5.3 Gyr for the 4$-$7 Gyr range, $\pm$6.13 Gyr for ages between 7$-$12 Gyr, and $\pm$0.1 dex for metallicity. Additionally, these errors represent an upper limit of the actual error, as our spectra always have a signal such that S/N $\geq$ 15, and the errors are determined for S/N = 10.

iii. We have obtained 21 maps associated with the age and metallicity of each of the galaxies considered in this work, allowing us to infer their age-metallicity plane for each of the spaxels comprising the sample. Only for 5 out of the 21 galaxies, the stellar populations for the entire bulge could not be reproduced due to low signal-to-noise ratio (S/N $<$ 15 for regions contained within the bulge effective radius considered in Zarattini et al. (in preparation)).

iv. We presented a detailed discussion of the galaxies NGC 5962, NGC 4405, and NGC 1087 to illustrate the analysis and interpretation of results we have done for the full sample of 21 galaxies. All three show a good fit to the data, although for NGC 5962, the signal-to-noise ratio is quite high, ensuring greater reliability of the data.

v. NGC 5962 exhibits a young stellar population ($\sim$ 3.5 $\pm$ 1 Gyr) with a metallicity fairly close to solar (0.04 $\pm$ 0.1 dex) for the central region, while surrounding the bulge, an annular structure with even younger populations ($\sim$ 1 $\pm$1 Gyr) and varying metallicities is observed, increasing their values from the inside out ($-$0.4, 0.2 dex).

vi. NGC 4405 has a younger central bulge compared to its surroundings (2, 2.5$\pm$1 Gyr) with low metallicity ($\sim$ 0.1, 0.2$\pm$0.1 dex).

vii. NGC 1087 is a star-forming galaxy, with a very young population of only 1$\pm$1 Gyr old and a very extended, but always low, metallicity. It lies between $-$1.4 and $-$0.4 $\pm$0.1 dex.

viii. Regarding the bulge formation scenario in these bulgeless sample of galaxies, it has been inferred through comparison with the CALIFA data discussed in de Lorenzo-Cáceres et al. (in preparation), that the stars composing the bulge are generally younger than expected for regular bulges of the same mass. This suggests that these are bulges formed from disc material, undergoing internal secular evolution and not resulting from merger processes. Furthermore, these bulges are enriched in metals from previous generations of stars.

From a technical point of view, this final master thesis reached its goals about introducing different astronomical data analysis tools.

i. I have expanded my knowledge of integral field spectrograph data processing. In particular, the treatment of MEGARA MR-G data.

ii. I have acquired knowledge about how to use the pPXF software for data processing by modifying the study parameters (wavelength ranges, regularisation factors, S/N ratio, etc.) These are the ones that have allowed me to carry out many tests before getting the final stellar population maps of the BEARD sample used in this project.

iii. I have learned to use and deal with star libraries and SSP models. In particular with the MILES models.

iv. I have been able to improve my skills with the Python tool, which has been essential for the development of the work.

As part of future work, it is proposed to extend the analysis to the entire BEARD galaxy sample that possesses MEGARA data, expanding the results from 21 galaxies to 53. This extension aims to calculate the mass-to-light ratio, enabling comprehensive comparisons with existing literature. Additionally, it is suggested to develop mock spectral models incorporating composite stellar populations to ensure consistent outcomes even in scenarios involving multiple starbursts. Moreover, the acquisition of [α/Fe] measurements within the spectral range of MEGARA is proposed, offering a deeper understanding of galactic evolution. Through these endeavours, the potential exists to publish an article highlighting the scientific achievements resulting from this project.

References

J Méndez-Abreu, A de Lorenzo-Cáceres, and SF Sánchez. The origin of bulges and discs in the califa survey–i. morphological evolution. *Monthly Notices of the Royal Astronomical Society*, 2021.

Edwin Hubble. *The Realm of Nebulae*. Yale University Press, New Haven, 1926.

Gerard De Vaucouleurs. General physical properties of external galaxies. *Astrophysik IV: Sternsysteme/Astrophysics IV: Stellar Systems*, 1959.

John Kormendy and Robert C Kennicutt Jr. Secular evolution and the formation of pseudobulges in disk galaxies. *Annu. Rev. Astron. Astrophys.*, 2004.

Alar Toomre. Mergers and some consequences. In *Evolution of Galaxies and Stellar Populations*, 1977.

Simon DM White and Martin J Rees. Core condensation in heavy halos: a two-stage theory for galaxy formation and clustering. *Monthly Notices of the Royal Astronomical Society*, 1978.

Ludwig Oser, Jeremiah P Ostriker, Thorsten Naab, Peter H Johansson, and Andreas Burkert. The two phases of galaxy formation. *The Astrophysical Journal*, 2010.

Luca Costantin, Jairo Méndez-Abreu, Enrico M Corsini, Lorenzo Morelli, Adriana de Lorenzo-Cáceres, Ilaria Pagotto, Virginia Cuomo, J Alfonso L Aguerri, and Michela Rubino. Dynamical structure of small bulges reveals their early formation in λcdm paradigm. *The Astrophysical Journal Letters*, 2020.

John Kormendy and Karl Gebhardt. Supermassive black holes in galactic nuclei. In *AIP conference proceedings*. American Institute of Physics, 2001.

John Kormendy and David B Fisher. Secular evolution in disk galaxies: Pseudobulge growth and the formation of spheroidal galaxies. *arXiv preprint arXiv:0810.2534*, 2008.

Cecilia Scannapieco, Simon DM White, Volker Springel, and Patricia B Tissera. The formation and survival of discs in a λcdm universe. *Monthly Notices of the Royal Astronomical Society*, 2009.

OJ Eggen, Donald Lynden-Bell, and AR Sandage. Evidence from the motions of old stars that the galaxy collapsed. *The Astrophysical Journal*, 1962.

Paola Di Matteo, Antonio Pipino, Matthew D Lehnert, Françoise Combes, and Benoit Semelin. On the survival of metallicity gradients to major dry-mergers. *Astronomy & Astrophysics*, 2009.

Michele Cappellari. Improving the full spectrum fitting method: Accurate convolution with gauss–hermite functions. *Monthly Notices of the Royal Astronomical Society*, 2017.

A Vazdekis, P Coelho, Santi Cassisi, E Ricciardelli, J Falcón-Barroso, Patricia Sánchez-Blázquez, F La Barbera, MA Beasley, and Adriano Pietrinferni. Evolutionary stellar population synthesis with miles–ii. scaled-solar and α-enhanced models. *Monthly Notices of the Royal Astronomical Society*, 2015.

T Ruiz-Lara, I Pérez, Carme Gallart, D Alloin, M Monelli, M Koleva, E Pompei, M Beasley, Patricia Sánchez-Blázquez, E Florido, et al. Recovering star formation histories: Integrated-light analyses vs. stellar colour–magnitude diagrams. 2015.

T Ruiz-Lara, MA Beasley, J Falcón-Barroso, J Román, F Pinna, C Brook, A Di Cintio, I Martín-Navarro, I Trujillo, and A Vazdekis. Spectroscopic characterization of the stellar content of ultra-diffuse galaxies. *Monthly Notices of the Royal Astronomical Society*, 2018.

Robert C Kennicutt Jr, François Schweizer, and Joshua E Barnes. *Galaxies: Interactions and Induced Star Formation: Saas-Fee Advanced Course 26. Lecture Notes 1996 Swiss Society for Astrophysics and Astronomy*. Springer Science & Business Media, 1998.

Charlie Conroy. Modeling the panchromatic spectral energy distributions of galaxies. *Annual Review of Astronomy and Astrophysics*, 2013.

Gustavo Bertelli, A Bressan, Ci Chiosi, F Fagotto, and E Nasi. Theoretical isochrones from models with new radiative opacities. *As-*

tronomy and Astrophysics Supplement Series, 1994.

Paola Marigo, Léo Girardi, Alessandro Bressan, Martin AT Groenewegen, Laura Silva, and Gian Luigi Granato. Evolution of asymptotic giant branch stars-ii. optical to far-infrared isochrones with improved tp-agb models. *Astronomy & Astrophysics*, 2008.

Adriano Pietrinferni, Santi Cassisi, Maurizio Salaris, and Fiorella Castelli. A large stellar evolution database for population synthesis studies. i. scaled solar models and isochrones. *The Astrophysical Journal*, 2004.

G Schaller, D Schaerer, G Meynet, and A Maeder. New grids of stellar models from 0.8 to 120 solar masses at z= 0.020 and z= 0.001. *Astronomy and Astrophysics Supplement Series*, 1992.

Aaron Dotter, Brian Chaboyer, Darko Jevremović, Veselin Kostov, E Baron, and Jason W Ferguson. The dartmouth stellar evolution database. *The Astrophysical Journal Supplement Series*, 2008.

Don A VandenBerg and R Acite Bell. Theoretical isochrones for globular clusters with predicted bvri and stromgren photometry. *The Astrophysical Journal Supplement Series*, 1985.

Don A VandenBerg, Peter A Bergbusch, and Patrick D Dowler. The victoria-regina stellar models: evolutionary tracks and isochrones for a wide range in mass and metallicity that allow for empirically constrained amounts of convective core overshooting. *The Astrophysical Journal Supplement Series*, 2006.

Edwin E Salpeter. The luminosity function and stellar evolution. *The Astrophysical Journal*, 1955.

John M Scalo. The stellar initial mass function. *Fundamentals of cosmic physics*, 11:1–278, 1986.

Pavel Kroupa. On the variation of the initial mass function. *Monthly Notices of the Royal Astronomical Society*, 2001.

Gilles Chabrier. Galactic stellar and substellar initial mass function1. *Publications of the Astronomical Society of the Pacific*, 2003.

Alister W Graham and Simon P Driver. A concise reference to (projected) sérsic r1/n quantities, including concentration, profile slopes, petrosian indices, and kron magnitudes. *Publications of the Astronomical Society of Australia*, 2005.

A Gil de Paz, E Carrasco, J Gallego, FM Sánchez, JM Vílchez Medina, ML García-Vargas, X Arrillaga, MA Carrera, A Castillo-Morales, E Castillo-Domínguez, et al. Megara: the future optical ifu and multi-object spectrograph for the 10.4 m gtc telescope. In *Ground-based and Airborne Instrumentation for Astronomy IV*. SPIE, 2012.

A Gil de Paz, E Carrasco, J Gallego, J Iglesias-Páramo, R Cedazo, ML García Vargas, Xabier Arrillaga, José L Avilés, Nicolás Cardiel, MA Carrera, et al. Megara, the new intermediate-resolution optical ifu and mos for gtc: getting ready for the telescope. In *Ground-based and Airborne Instrumentation for Astronomy VI*. SPIE, 2016.

M Chamorro-Cazorla, A Gil de Paz, Á Castillo-Morales, J Gallego, E Carrasco, J Iglesias-Páramo, ML García-Vargas, S Pascual, N Cardiel, C Catalán-Torrecilla, et al. Megades: Megara galaxy disc evolution survey-data release i: Central fields. *Astronomy & Astrophysics*, 2023.

Michele Cappellari and Yannick Copin. Adaptive spatial binning of integral-field spectroscopic data using voronoi tessellations. *Monthly Notices of the Royal Astronomical Society*, 2003.

Michele Cappellari and Eric Emsellem. Parametric recovery of line-of-sight velocity distributions from absorption-line spectra of galaxies via penalized likelihood. *Publications of the Astronomical Society of the Pacific*, 2004.

I Millán-Irigoyen, M Mollá, M Cerviño, Y Ascasibar, ML García-Vargas, and PRT Coelho. Hr-pypopstar: high-wavelength-resolution stellar populations evolutionary synthesis model. *Monthly Notices of the Royal Astronomical Society*, 2021.

Gary J Ferland, WJ Henney, CR O'Dell, RL Porter, PAM Van Hoof, and RJR

Williams. Pumping up the [n i] nebular lines. *The Astrophysical Journal*, 2012.

J-F Le Borgne, G Bruzual, R Pelló, A Lançon, B Rocca-Volmerange, B Sanahuja, D Schaerer, C Soubiran, and R Vílchez-Gómez. Stelib: A library of stellar spectra at. *Astronomy & Astrophysics*, 2003.

Patricia Sánchez-Blázquez, RF Peletier, Jorge Jiménez-Vicente, Nicolas Cardiel, A Javier Cenarro, Jesus Falcon-Barroso, Javier Gorgas, Selim Selam, and Alexandre Vazdekis. Medium-resolution isaac newton telescope library of empirical spectra. *Monthly Notices of the Royal Astronomical Society*, 2006.

J Falcón-Barroso, P Sánchez-Blázquez, A Vazdekis, E Ricciardelli, N Cardiel, AJ Cenarro, J Gorgas, and RF Peletier. An updated miles stellar library and stellar population models. *Astronomy & Astrophysics*, 2011.

Ph Prugniel and Caroline Soubiran. A database of high and medium-resolution stellar spectra. *Astronomy & Astrophysics*, 2001.

Renbin Yan, Yanping Chen, Daniel Lazarz, Dmitry Bizyaev, Claudia Maraston, Guy S Stringfellow, Kyle McCarthy, Sofia Meneses-Goytia, David R Law, Daniel Thomas, et al. Sdss-iv mastar: a large and comprehensive empirical stellar spectral library—first release. *The Astrophysical Journal*, 2019.

Yan-Ping Chen, SC Trager, RF Peletier, A Lançon, A Vazdekis, Ph Prugniel, DR Silva, and A Gonneau. The x-shooter spectral library (xsl)-i. dr1: Near-ultraviolet through optical spectra from the first year of the survey. *Astronomy & Astrophysics*, 2014.

Kristiina Verro, SC Trager, RF Peletier, A Lançon, A Gonneau, A Vazdekis, Philippe Prugniel, Y-P Chen, PRT Coelho, P Sánchez-Blázquez, et al. The x-shooter spectral library (xsl): Data release 3. *Astronomy & Astrophysics*, 2022.

Adriano Pietrinferni, Marco Molinaro, Santi Cassisi, Fabio Pasian, Maurizio Salaris, Danilo Pelusi, Patrizia Manzato, and Claudio Vuerli. Basti: An updated, advanced and vo-compliant database of stellar evolution predictions. *Astronomy and Computing*, 2014.

M. Cappellari. Full spectrum fitting with photometry in ppxf: non-parametric star formation history, metallicity and the quenching boundary from 3200 LEGA-C galaxies at redshift $z \approx 0.8$. *MNRAS submitted*, 2022. doi: 10.48550/arXiv.2208.14974.

R Brent Tully, Edward J Shaya, Igor D Karachentsev, Hélene M Courtois, Dale D Kocevski, Luca Rizzi, and Alan Peel. Our peculiar motion away from the local void. *The Astrophysical Journal*, 2008.

Michele Cappellari, Eric Emsellem, Davor Krajnović, Richard M McDermid, Nicholas Scott, GA Verdoes Kleijn, Lisa M Young, Katherine Alatalo, R Bacon, Leo Blitz, et al. The atlas3d project–i. a volume-limited sample of 260 nearby early-type galaxies: science goals and selection criteria. *Monthly Notices of the Royal Astronomical Society*, 2011.

Jeremy R Mould, John P Huchra, Wendy L Freedman, Robert C Kennicutt Jr, Laura Ferrarese, Holland C Ford, Brad K Gibson, John A Graham, Shaun MG Hughes, Garth D Illingworth, et al. The hubble space telescope key project on the extragalactic distance scale. xxviii. combining the constraints on the hubble constant. *The Astrophysical Journal*, 2000.

Sebastián F Sánchez, Rubén García-Benito, Stefano Zibetti, CJ Walcher, B Husemann, MA Mendoza, L Galbany, J Falcón-Barroso, D Mast, J Aceituno, et al. Califa, the calar alto legacy integral field area survey-iv. third public data release. *Astronomy & Astrophysics*, 2016a.

J Méndez-Abreu, SF Sánchez, and A de Lorenzo-Cáceres. Spectro-photometric decomposition of galaxy structural components. *Monthly Notices of the Royal Astronomical Society*, 2019.

SF Sánchez, E Pérez, P Sánchez-Blázquez, JJ González, FF Rosález-Ortega, M Cano-Díaz, C López-Cobá, RA Marino, A Gil de Paz, M Mollá, et al. Pipe3d, a pipeline to analyze integral field spectroscopy data: I. new fitting philosophy of fit3d. *Revista mexicana de astronomía y astrofísica*, 2016b.

Appendices

Appendix A: Stellar population maps

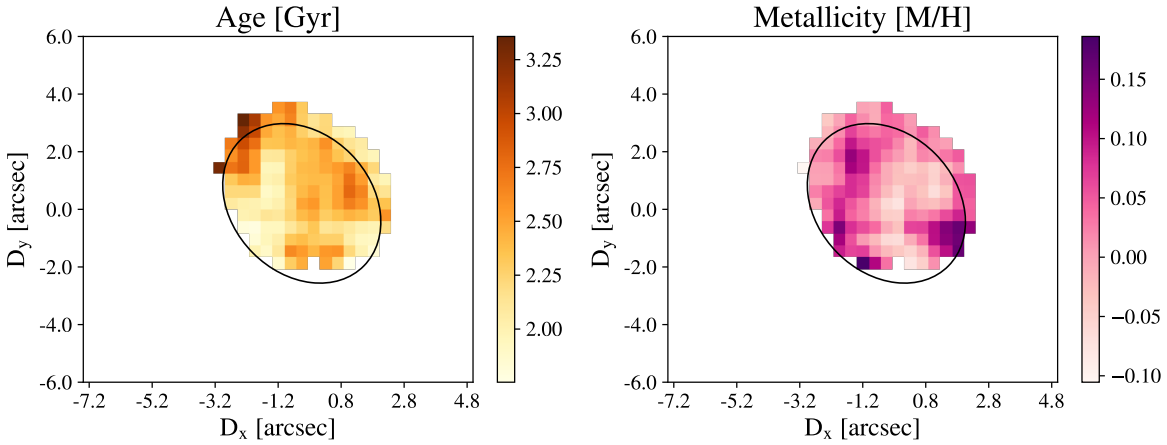

Figure A.1: IC 3392

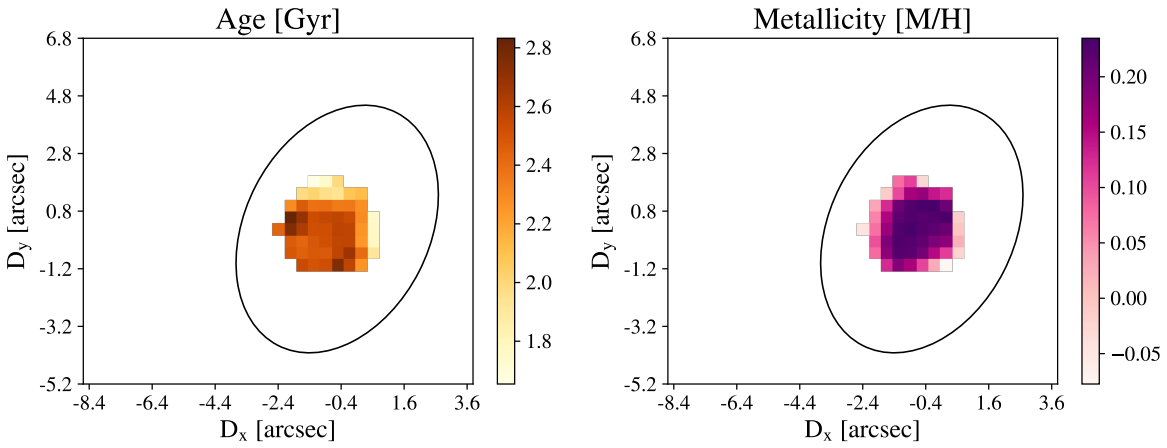

Figure A.2: NGC 0514

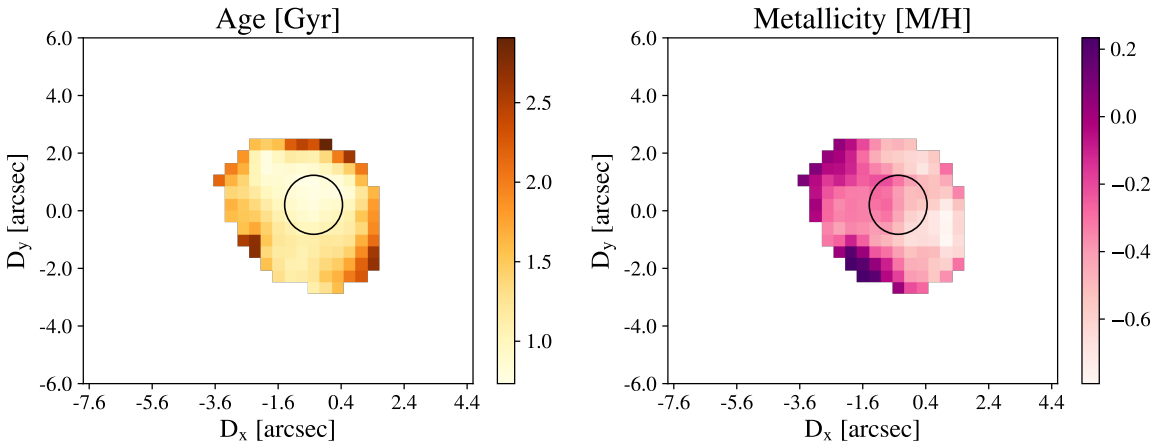

Figure A.3: NGC 2543

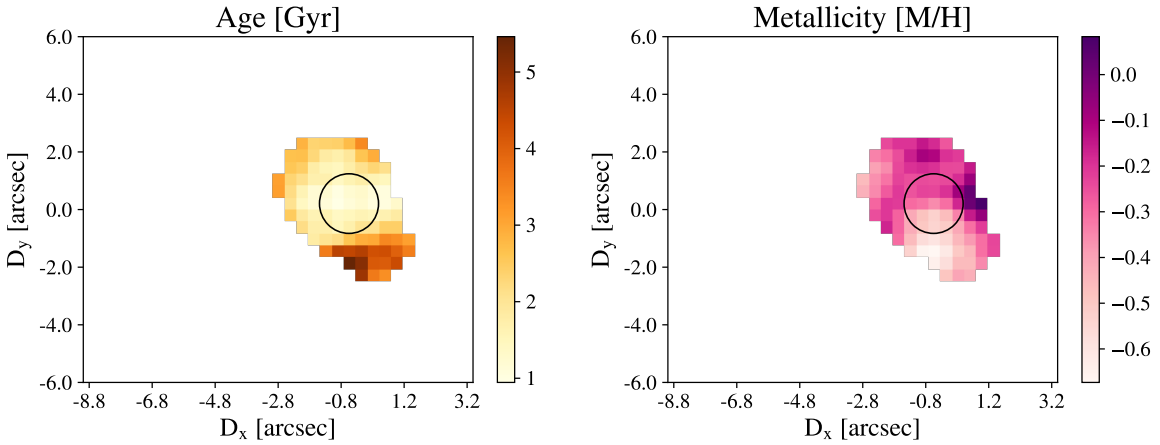

Figure A.4: NGC 2701

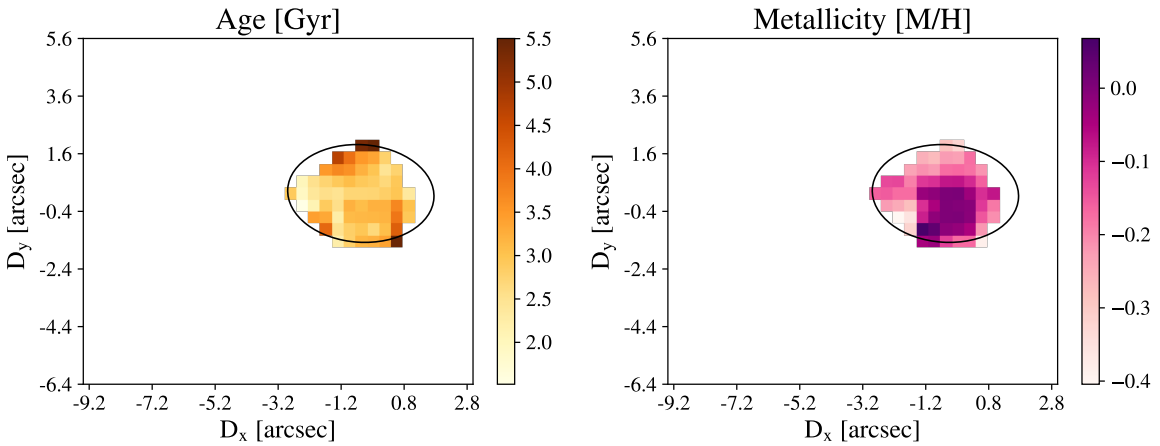

Figure A.5: NGC 2742

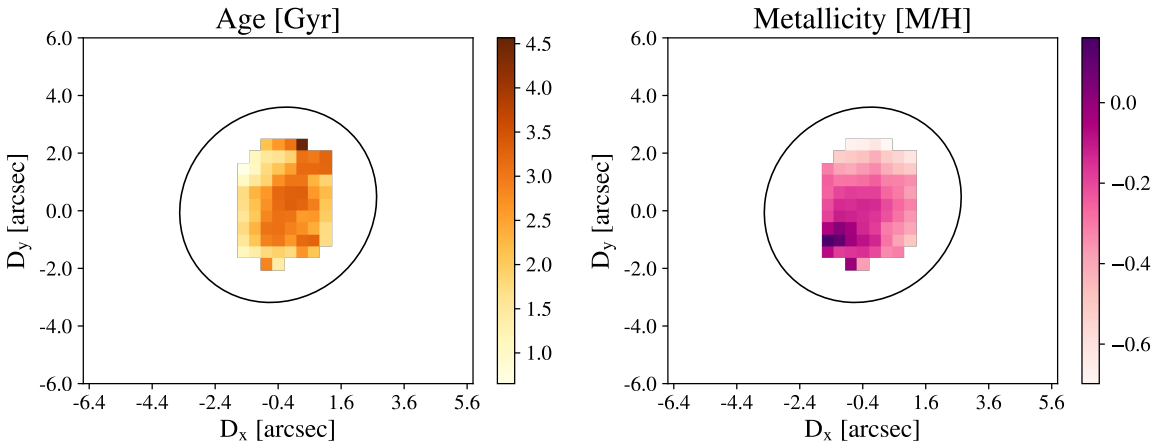

Figure A.6: NGC 2776

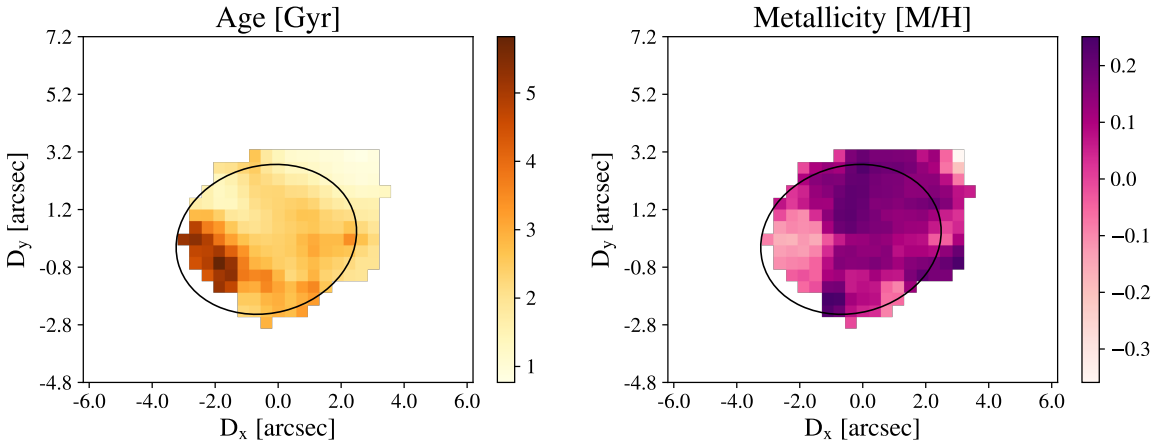

Figure A.7: NGC 3294

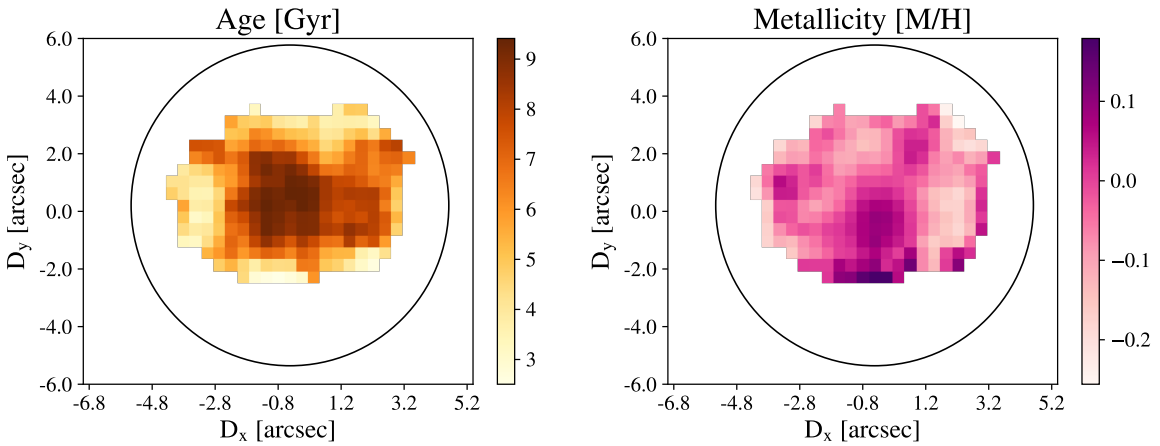

Figure A.8: NGC 3338

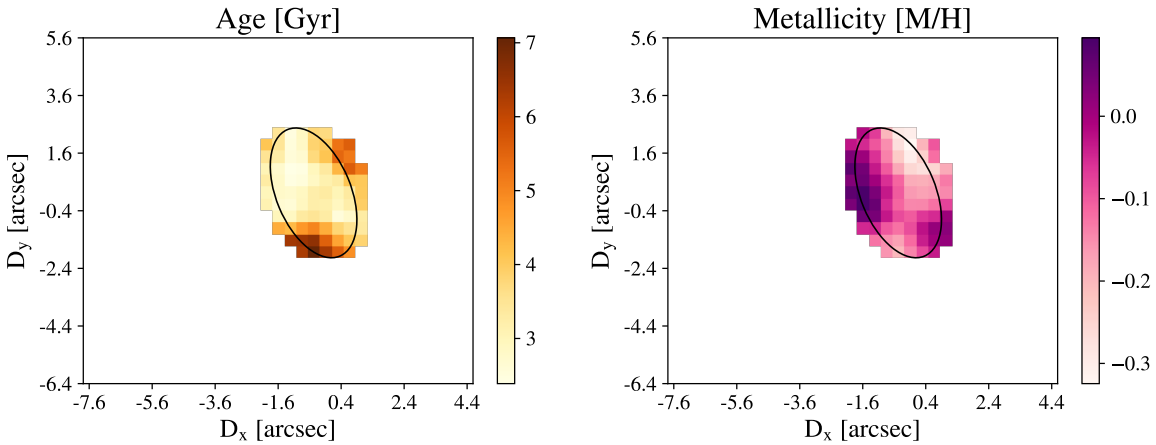

Figure A.9: NGC 3430

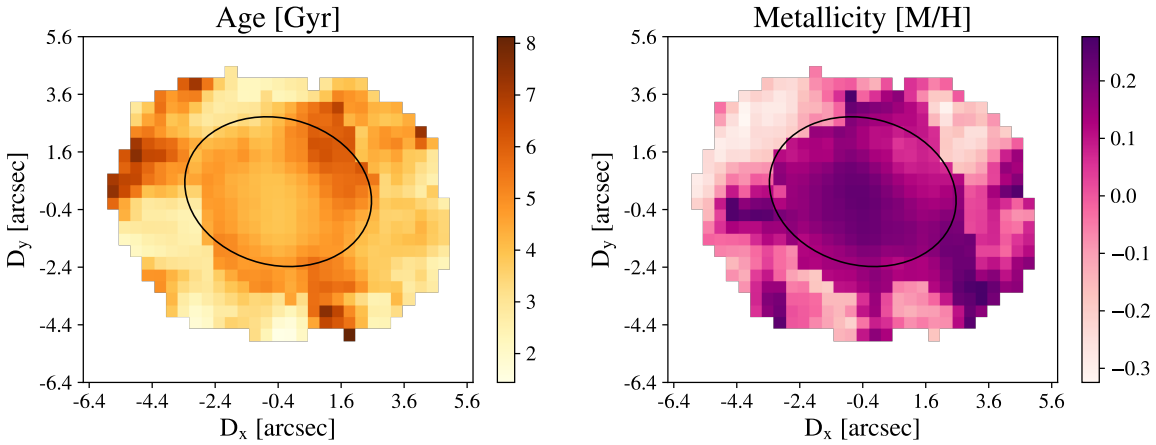

Figure A.10: NGC3486

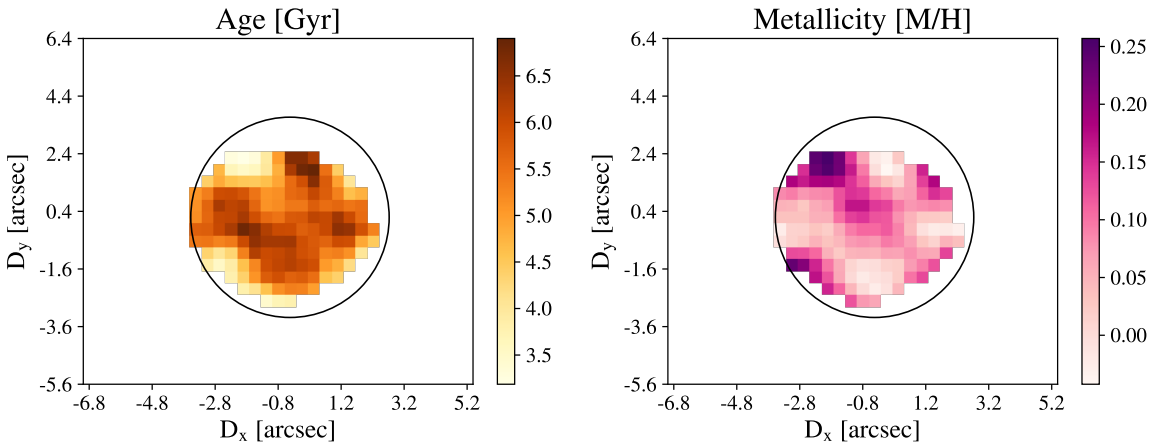

Figure A.11: NGC 3780

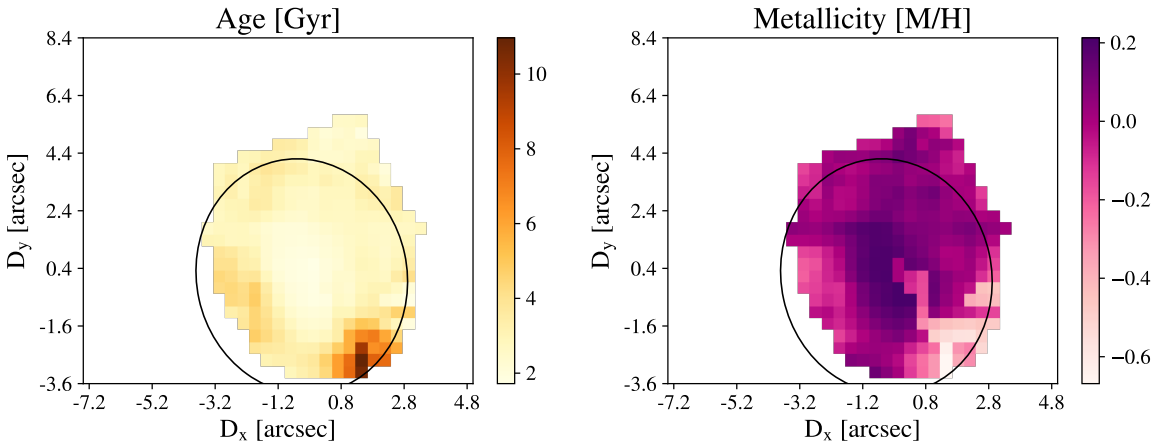

Figure A.12: NGC 3810

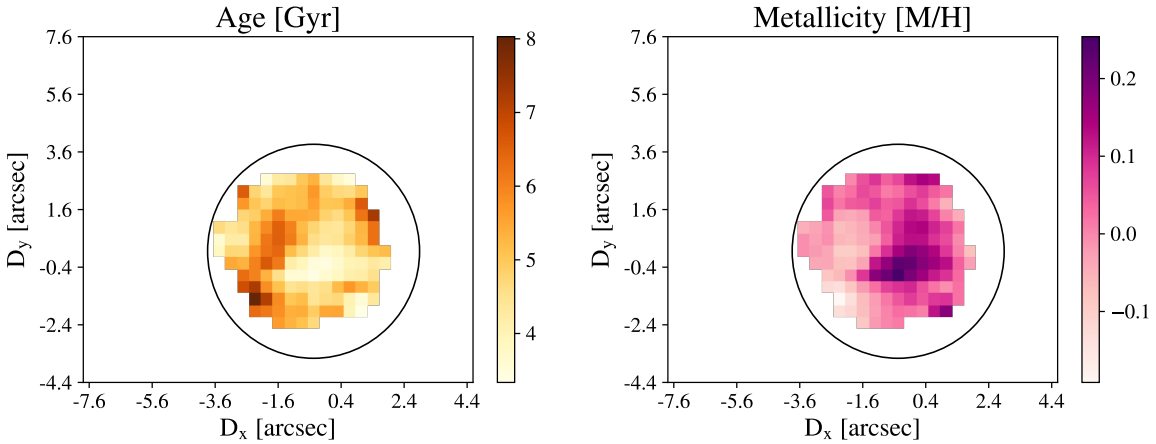

Figure A.13: NGC 3938

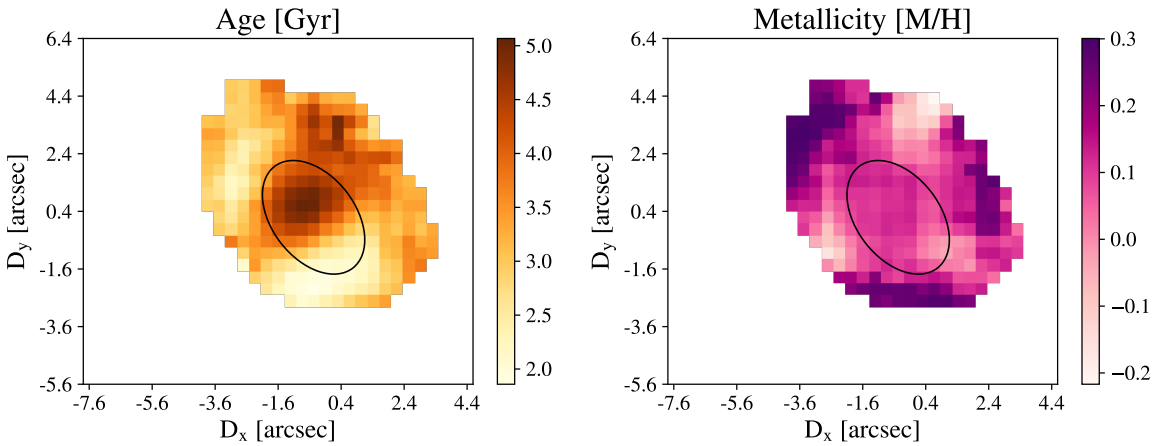

Figure A.14: NGC 5313

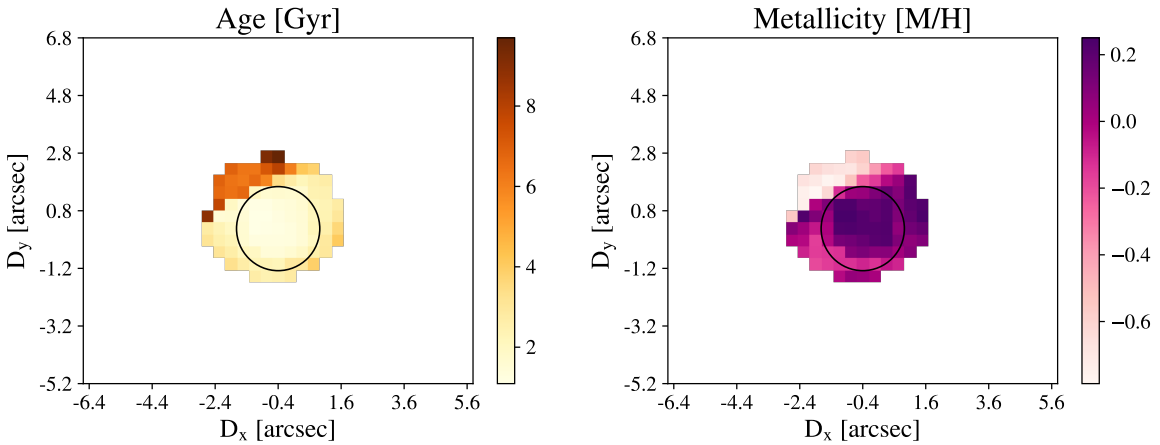

Figure A.15: NGC 5347

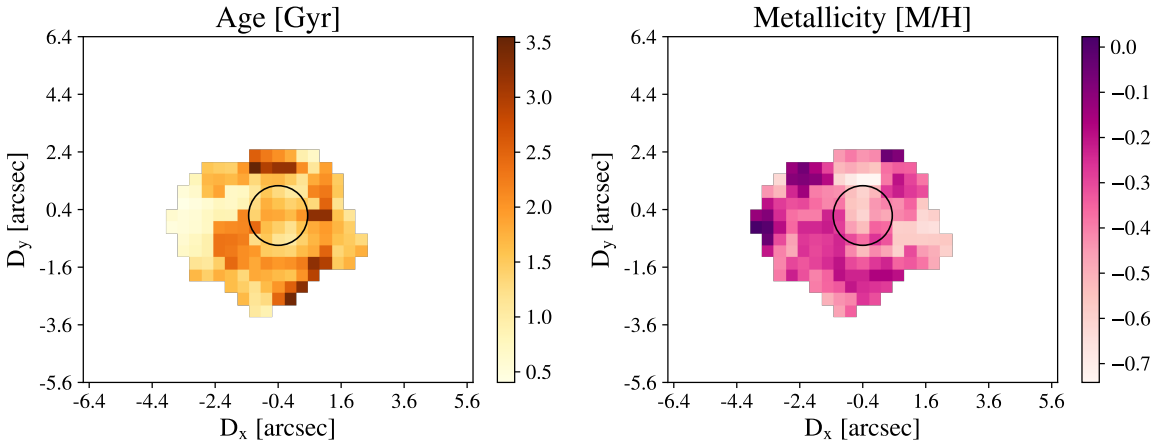

Figure A.16: NGC 5633

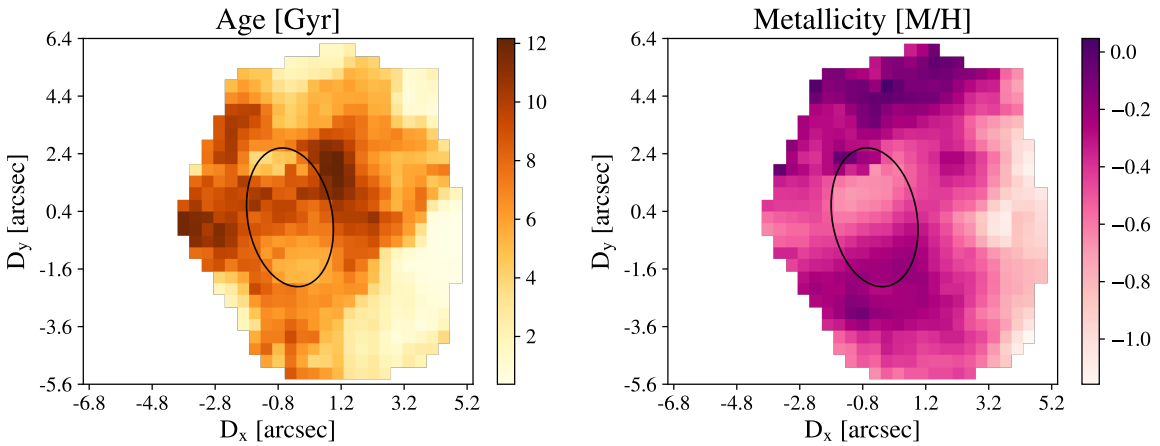

Figure A.17: NGC 5899

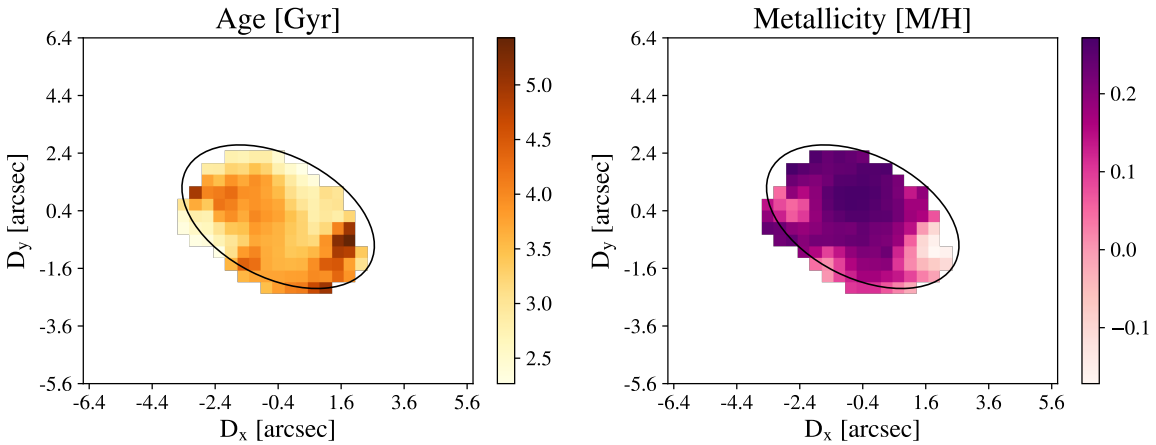

Figure A.18: NGC 6070